Article:
Moysa, A, Steczkiewicz, K, Niedzialek, D et al. (4 more authors) (2021) A model of full-length RAGE in complex with S100B. Structure, 29 (9). pp. 989-1002. ISSN 0969-2126

https://doi.org/10.1016/j.str.2021.04.002

A model of full-length RAGE in complex with S100B

Alexander Moysa[1]*, Kamil Steczkiewicz[2]*, Dorota Niedzialek[2], Dietmar Hammerschmid[3,5], Lilia Zhukova[2], Frank Sobott[4,5], Michal Dadlez[2]

Author information
[1,2]Institute of Biochemistry and Biophysics, PAS, Pawinskiego 5a, 02-109 Warsaw, Poland.
[3]Department of Chemistry, King's College London, 7 Trinity Street, SE1 1DB, London, UK
[4]Astbury Centre for Structural Molecular Biology and School of Molecular and Cellular Biology, University of Leeds, Woodhouse Lane, LS2 9JT Leeds, UK.
[5]Department of Chemistry, Biomolecular & Analytical Mass Spectrometry group, University of Antwerp, Antwerp, Belgium, Groenenborgerlaan 171, 2020, Antwerp, Belgium
*Corresponding authors: a.alexandrmoysa@gmail.com (A.M.), ksteczk@ibb.waw.pl (K.S.)
[1]Lead Contact
*Correspondence: a.alexandrmoysa@gmail.com (A.M.)

Summary

The Receptor for Advanced Glycation End-products (RAGE) is an immunoglobulin-type multiligand transmembrane protein expressed in numerous cell types, including the central nervous system cells. RAGE interaction with S100B, released during brain tissue damage, leads to RAGE upregulation and initialization of a spiral proinflammatory associated with different neural disorders. Here, we present the structural characterization of the hetero-oligomeric complex of the full-length RAGE with S100B, obtained by a combination of mass spectrometry-based methods and molecular modelling. We predict that RAGE functions as a tightly packed tetramer exposing a positively charged surface formed by V domains for S100B binding. Based on HDX results we demonstrate an allosteric coupling of the distal extracellular V-domains and the transmembrane region, indicating a possible mechanism of signal transmission by RAGE across the membrane. Our model provides an insight into RAGE-ligand interactions, providing a basis for the rational design of the therapeutic modifiers of its activity.

Introduction

RAGE is a multi-domain transmembrane protein, structurally related to the family of immunoglobulins. It was initially characterized as a receptor for advanced glycation end products (AGEs) (Neeper et al., 1992), hence its name, but it was later shown to recognize a considerable variety of Damage-Associated Molecular Pattern molecules (DAMPs). Upon accepting a ligand, RAGE transduces the signal across the cell membrane, triggering a pro-inflammatory cellular response. The signal transduction process is closely linked to the oligomerization status of RAGE (Xu et al., 2013; Wei et al., 2012; Yatime et al., 2013). The RAGE signalling pathway is associated with multiple chronic diseases like diabetes (Moldogazieva et al., 2019), peripheral neuropathy (Park et al., 2014), cardiovascular disorders (S. F. Yan, Ramasamy, and Schmidt 2009), chronic inflammations (Riehl et al., 2010), cancer (Yin et al., 2013; Taub et al., 2019), and neurodegeneration (MacLean et al., 2019; Zhang et al., 2014; Fang et al., 2010; Juranek et al., 2016), all of which render it as a critically important potential drug target. However, despite significant efforts, a comprehensive understanding of the structure of RAGE-ligand complexes and the molecular mechanism of signal transduction are still elusive.

RAGE consists of three extracellular (Ig)-like domains, named: V, C1 and C2, which are followed by a single transmembrane helix (TM) and a short cytoplasmic tail (CT) forming a signalling domain . The cytoplasmic tail of RAGE shares no homology with other receptor cytoplasmic domains and does not provide tyrosine kinase activity (Hudson et al., 2008). It has been established before that the V and C1 domains form a structural and functional unit, which is connected to the C2 domain through a flexible linker (Yatime et al., 2013; Yatime et al., 2016). The extracellular part of the receptor has multiple patches of hydrophobic or charged residues suitable for specific interaction with ligands. However, there is growing evidence that also oligomerization of RAGE plays a major role in ligand binding (Xu et al., 2013; Ostendorp et al., 2007; Xue et al., 2016; Koch et al., 2010; Yatime et al., 2016; Xie et al., 2007). Due to flexibility of the C1-C2 linker, the ligand-binding sites at V or C1 domains are structurally uncoupled from the TM region, therefore signal transduction is thought to be mediated by RAGE oligomerization patterns.

The wide ensemble of RAGE ligands, aside from AGEs (Xue et al., 2011), includes the high mobility group box-1 protein (Huttunen et al., 2002), amyloid-β peptide (Yan et al., 1998), S100 proteins (Huttunen et al., 2000; Leclerc et al., 2009) and even nucleic acid chains (Yatime et al., 2014). The S100 protein family consists of more than 20 members of calcium-binding proteins (Donato et al., 1999). The most studied member of this family is S100B protein, which exhibits neurotoxic activity mediated by the interaction with RAGE (Sedaghat et al., 2008; Leclerc et al., 2010; Villarreal et al., 2014; Michetti et al., 2019). Complexes of S100B with extracellular fragments of RAGE were the focus of earlier structural studies (Ostendorp et al., 2007; Xue et al., 2016; Koch et al., 2010), but no consensus has been reached even as to their oligomeric status. For instance, Ostendorp and co-authors proposed symmetrical parallel dimerization of RAGE, where S100B tetramer interacts with dimerized V domains (pdb|2h61) (Ostendorp et al., 2007). On the other hand, Xue and co-authors noticed that the V domain is highly positively charged which would prevent V domains from immediate dimerization and, instead, suggested an asymmetrical mode of the RAGE dimerization, guided by the interaction between negatively charged C2 domain and the positively charged VC1 module (Xue et al., 2016). Although full structural information about RAGE-S100B interaction is still missing, two structures showed how S100B interacts with fragments of the V domain (pdb|4xyn (Jensen et al., 2015) and pdb|5d7f).

An X-ray structure of the extracellular part of RAGE (exRAGE) (pdb|4ybh) demonstrated spatial relationships between V, C1 and C2 domains (Yatime et al., 2016). For instance, it revealed that V and C1 domains are rather tightly connected with a short linker, while the C2 domain remains loosely connected to C1 through a linker allowing for freedom in their relative orientation. An NMR structure of RAGE C-terminal domain (CT, pdb|2lmb) showed that the major part of it is mostly disordered *in vivo,* and interaction with its cytoplasmic partner Protein diaphanous homolog 1 (DIAPH1) is more complex than one-to-one binding and might include structural changes in both RAGE and DIAPH1 (Rai et al., 2012).

Structural studies based on X-ray crystallography or NMR of the full-length RAGE (FL_RAGE) are hampered due to the challenges inherent for oligomerizing membrane protein systems. Truncations of the FL_RAGE are more feasible for conventional approaches, but these modifications may affect the binding patterns or change the oligomerization properties of the receptor. The cryo-EM approach is more promising here, but despite spectacular improvement in the determination of three-dimensional structures of proteins, membrane proteins still represent a significant challenge for this technique (Cheng et al., 2018). In our previous paper, we showed that alternative methods of structure analysis may bring insight into the properties of FL-RAGE and its oligomeric distributions (Moysa et al., 2019). Therefore, in the present work, we extended this study to analyze the structural properties of FL_RAGE-S100B complexes using a combination of mass spectrometry-based methods with molecular modelling.

Results

Native MS - Stoichiometry

Subunit stoichiometry is believed to be crucial for the FL_RAGE-S100B complex and its function. The information on stoichiometry reveals the oligomerization status of the complex and thus provides valuable constraint information for rational modelling. To study the stoichiometry of FL_RAGE-S100B, we subjected both FL_RAGE and S100B individually, as well as in complex to native mass spectrometry (native MS) (Leney et al., 2017).

S100B exhibits intrinsic oligomerization tendencies with a predominance of homo-dimerization (Thulin et al., 2011). Binding of calcium to S100B has been shown to induce a conformational change, leading to the exposure of the binding site to target proteins (Smith et al., 1998). Moreover, calcium also influences the oligomerization status of the proteins' homocomplex formation (Ostendorp et al., 2007). Therefore, to study the effect of calcium, we aimed to interrogate S100B in the presence and absence of $CaCl_2$. As expected, the apo sample, i.e. no $CaCl_2$ added, predominantly shows dimers, although tetrameric and hexameric complexes have been observed as well (Fig. 1A). Yet, the addition of $CaCl_2$ (200 µM) shifts this equilibrium towards higher-order oligomeric species with dimeric, tetrameric, hexameric, and even octameric species present (Fig. 1B). The peak broadening observed upon $CaCl_2$ addition originates from Ca-adduct formation. Lower concentrations of $CaCl_2$, however, do not lead to stronger S100B oligomerization (data not shown). The effect of a Ca-induced oligomerization of S100B has previously also been observed by Ostendorp (Ostendorp et al., 2007). Collisional activation of S100B leads, as expected, to the dissociation of homo-oligomeric complexes into monomers (Fig. 1C).

The transmembrane helix of RAGE requires a membrane mimicking environment for solubility, which is needed for characterization of the properties of the full-length protein. Therefore, we purified and solubilized FL_RAGE in Triton X-100 detergent micelles at two times the critical micelle concentration (CMC) for native MS analysis. The oligomeric species identified are identical with what has previously been observed (Moysa et al., 2019), ranging from monomeric up to tetrameric complexes (Fig. 1D). The different oligomeric forms display a narrow charge state distribution which indicates the native character of these complexes, suggesting that no substantial unfolding and/or dissociation occurred during the MS experiment. A 1:5 mixture of FL_RAGE and S100B, however, exhibits a more complex spectrum of different stoichiometries with a prevalence of trimer(FL_RAGE)-dimer(S100B) and dimer(FL_RAGE)-dimer(S100B) heterooligomers (Fig. 1E). As compared to the FL_RAGE analysis, monomeric species of FL_RAGE show a much broader charge state distribution with higher charged species observed. Additionally, monomeric S100B complexes are present which were observed only in collision-activated (Fig. 1C) but not in native measurements of S100B (Fig. 1A, B), indicating the dissociation of S100B oligomers and FL_RAGE-S100B complexes caused by high levels of collision energy required for releasing the complexes from detergent micelles. Thus, to distinguish between native, solution-phase complexes, and dissociation products, we have to compare the charge states of FL_RAGE and FL_RAGE-S100B in more detail (Fig. 1D, E). The representative charge envelopes for trimer(FL_RAGE)-dimer(S100B) (+29 - +24) and dimer(FL_RAGE)-dimer(S100B) (+24 - +21) exhibit an average increase in charge state of ~+5 for two additional S100B subunits relative to trimeric (+25 - +18) and dimeric (+20 - +15) FL_RAGE. By contrast, complexes which contain one S100B subunit, e.g. trimer(FL_RAGE)-monomer(S100B) (+21 - +19) and dimer(FL_RAGE)-monomer(S100B) (+17 - +14), do not show such an increase in charge state, i.e. lower number of charges than expected, and thus clearly pointing at a dissociation process. Species containing monomeric S100B are thus the complex dissociation artefacts. This observation is further supported by a much broader charge state envelope for monomeric FL_RAGE and the presence of monomeric S100B in the complex sample.

Obviously, binding of S100B to FL_RAGE leads to complexes of different stoichiometries. However, results indicate that S100B participates in the complex as a homooligomer with an even number of subunits, e.g. dimer or tetramer, rather than as monomer. Even though we could not find a tetrameric S100B unit bound to FL_RAGE, previous studies have shown that S100B binds with higher affinity as a tetramer compared to a dimer (Ostendorp et al., 2007). The reason for lacking complexes with tetrameric S100B binding might be that physiological conditions, i.e. 3 mM $CaCl_2$ (Hurwitz et al., 1996) are hardly feasible in MS due to massive ion suppression and adduct formation (Donnelly et al., 2019), or insufficient stabilization by the detergent micelle. Considering these circumstances, we decided to construct a model of tetrameric FL_RAGE in complex with tetrameric S100B. Other variants of RAGE-S100B complexes can be obtained by the decomposition of this model.

Chemical cross-linking - contact networks

Cross-linking coupled with mass spectrometry (XL-MS) has emerged as a powerful tool for examining protein-protein interactions. Data obtained in the course of XL-MS analysis provide spatial constraints that enable the modelling of protein complex structures and regions of interaction (Yu et al., 2018). In order to obtain experimental constraints crucial for the selection of a reliable model, we applied XL-MS on both FL_RAGE and FL_RAGE-S100B. Overall, we identified 27 and 39 cross-linked peptides in FL_RAGE and FL_RAGE-S100B samples, respectively (Supplementary Table S1). Of these, 13 and 16 cross-links account for intramolecular links in FL_RAGE oligomers and FL_RAGE-S100B complexes, respectively (Fig. 2A, also see details Materials and Methods). Upon S100B binding, the intra-protein cross-linking pattern remained unchanged within the C1 domain but was altered within the V domain. After the binding of S100B new intramolecular cross-links have emerged: Lys62 - Ser74, Lys52 - Lys62, Gly22-Lys39, Gly22-Lys62 while one disappeared: Gly22 - Ser111 (Fig. 2A). Since it has previously been shown that the binding of S100B to RAGE occurs through the V domain (Koch et al., 2010), observed rearrangement of intramolecular links may reflect structural changes in the V domain upon ligand binding. Also, in agreement with previous studies, 9 RAGE-S100B intermolecular links connected the V domain of RAGE with S100B (Fig. 2B). Further 14 RAGE-RAGE intermolecular links in FL_RAGE oligomers and 13 in FL_RAGE-S100B complexes were observed among the following domains: V-V, V-C1, C1-C1, and CT-CT (Supplementary Table S1 and Fig. 2B). The presence of multiple interaction contact surfaces demonstrates the participation of all domains in RAGE oligomerization which is in agreement with previous results (Moysa et al., 2019). Also, it renders a rather complex picture of the oligomerization process. Despite some alterations, the overall cross-linking pattern of RAGE-RAGE intermolecular links is maintained upon S100B binding, suggesting that the RAGE structure and arrangement in full FL_RAGE-S100B complex does not deviate much from oligomers spontaneously formed between FL_RAGE subunits.

3D modelling of complexes

Molecular modelling of the FL_RAGE oligomers and RAGE-S100B complexes carried out in this work integrates information from several sources: known 3D structures, native MS and XL-MS data and computational predictions. The necessity to combine data from different approaches in the process of modelling a complex of unknown structure and mechanism of action excluded the choice of the universal method for model building but rather imposed the strategy of splitting the modelling process into several conceptual stages.

Using only the cross-linking data as a sole guide for constructing RAGE oligomer does not immediately lead to an unambiguous oligomer assembly scheme. However, knowing that the RAGE and S100B interact as oligomers, we decided to organize the structure of FL_RAGE multimers using the known structure of S100B oligomers as a scaffold. Since the majority of intermolecular links have been found with V and C1 domains, and RAGE-S100B binding occurs via the V domain of RAGE, assembly of the model was initiated from a VC1 module interacting with S100B.

It is known that S100B is able to bind at least two distinct fragments of the V domain of RAGE (pdb|4xyn (Jensen et al., 2015) and pdb|5d7f) (Fig. 3A-B). Each S100B monomer can accommodate only one of the two RAGE fragments, imposing two distinct RAGE orientations at each site (Fig. 3C, D, E). That makes three variants of heterotetrameric RAGE-S100B (dimer (FL_RAGE) - dimer (S100B)): S100B binding “57-65” peptides at both sites or “70-79” peptides at both sites, or one site occupied by “57-65” peptide while the other by “70-79” peptide. However, the first and the third variants do not satisfy observed V-V and V-C1 cross-links, while the two "70-79” option is highly unlikely due to massive clashes between RAGE monomers and would require major structural rearrangements within both S100B dimer and RAGE VC1 domains. There is thus no way to pair S100B dimer with two molecules of RAGE without major perturbation of the dimer structure. Therefore, we turned to the possibilities offered by the structure of the S100B tetramer.

While binding sites of RAGE are located symmetrically within the S100B dimer (Fig. 3F), S100B tetramer (pdb|2h61 (Ostendorp et al., 2007)) organizes the RAGE dimers in such a way that two sites are located closer to each other (“central sites”) and two others are located more distantly (“peripheral sites”) (Fig. 3G). Because each of the 4 sites can bind either the "57-65" or "70-79" fragment, there are 10 unique combinations. However, only the variant in which “57-65” fragments occupy central sites and “70-79” fragments fit into peripheral sites of S100B tetramer, reconstructs all V-V and V-C1 intermolecular links and facilitates close location of C-terminal parts within the RAGE tetramer.

Since the native MS data demonstrated the presence of tetrameric RAGE, among the other oligomers, the heterooctamer (tetramer (FL_RAGE) - tetramer (S100B)) was selected for modelling. This heterooctamer was assembled in a two-step procedure. First, two dimers of S100B from pdb|4xyn and two dimers from pdb|5d7f were overlaid onto S100B tetrameric structure (pdb|2h61) to model S100B tetramer with four RAGE binding sites occupied by RAGE fragments (Fig. 3G). Eventually, four RAGE monomers (pdb|4ybh) were superimposed by the overlay of the corresponding peptides within the S100B tetramer, as shown in - (Fig. 3C, D). In this arrangement, two RAGE monomers contact the S100B tetramer occupying “central” binding sites and the other two “peripheral” sites. The overlay was followed up by both manual adjustments and energy minimization for a better fit, to obtain the final version of the heterooctamer (Fig. 4). C2 domains are connected to C1 through a 9 residue long flexible linker, which allows for the formation of a C2-tetramer at the RAGE oligomer central axis (Fig. 4). Nevertheless, both V and C1 domains, especially when oriented by the interaction with S100B tetramer, form almost rigid segments imposing constraints that limit the number of possible C2 orientations. We could not unambiguously determine whether C2 domains will dimerize, tetramerize or form another type of oligomer, so we decided on imposing tetramerization, corresponding to VC1 predicted tetramerization. The possibility of C2 tetramerization was shown in our previous study, where the C-terminal part of RAGE consisting of C2, TM and CT formed oligomers up to hexamer (Moysa et al., 2019). Each C2 domain buries the surface of 1022Å^2 within the modelled tetramer. The C2 tetramer is further connected to transmembrane helices via 20 amino acids linker of unknown structure. Those transmembrane helices oligomerize with also unknown stoichiometry, yet after assuming exRAGE tetramerization we assembled them into a four-helix bundle. Eventually, transmembrane helices connect with the C-terminal effector domain (CT) of the intracellular part of RAGE. The CT domain is mostly unstructured as a monomer (pdb|2lmb (Rai et al., 2012)) and might become more organized upon oligomerization and DIAPH1 binding (Manigrasso et al., 2016). *De novo* folding consistently predicted the formation of an alpha-helix right after the transmembrane element, and this alpha-helix might play an important role in the structuring of the CT domain.
Both the obtained model for heterooctameric FL_RAGE-S100B complex and for tetrameric FL_RAGE were critically assessed for compliance with observed cross-links (Fig. 5). Almost all unique links are reproduced by the model with only a few measured distances exceeding the threshold of 30Å (Supplementary Table S1). Such longer links might result from natural protein dynamics not captured by the model (Merkley et al., 2014).

A detailed comparison of RAGE-RAGE intermolecular links revealed differences related to S100B binding. The decreasing number of intermolecular links between V and C1 domains is caused by the introduction of new sites for cross-linking from S100B protein located in close proximity of V domains. S100B binding also caused a rearrangement of links between C1 domains, namely: the disappearance of Lys162-Lys162 and the appearance of Lys123-Lys162.

The resulting assembly is also consistent with work by Xue (Xue et al., 2016) who noticed that direct V-V interaction would be unfavorable due to their positive charges. In our model, interacting V domains are shifted along each other to avoid electrostatic repulsion but also to allow more tight fit within the 57-65 peptide binding site and between dimerizing VC1 modules themselves (contact surface of between central VC1 fragments is 2227Å^2. The C1 domain is also mildly negatively charged, to accept the positively charged V domain (Fig. 6A). Moreover, two VC1 domains interacting in such a way form a clear positively charged patch on dimer's surface, presumably for efficient binding of negatively charged ligands like S100B (Fig. 6B). The "central" VC1 domains together with "peripheral" modules form an extensive pocket burying a total buried surface area of 4514Å^2 between RAGE and S100B tetramers. For additional verification, the model has been subjected to exhaustive molecular dynamics simulations and remained stable, as described below.

HDX-MS - Changes in molecular dynamics of FL_RAGE upon binding S100B

To study ligand-induced changes in the structural dynamics landscape of FL_RAGE we used hydrogen-deuterium exchange mass spectrometry (HDX-MS). A comparison of H/D exchange patterns between the ligand-free and S100B-bound forms (Fig. 7) revealed two main regions of significant changes in the level of deuterium uptake. Firstly, the V domain shows a region of decreased protection which is in close proximity to the interaction interface between RAGE and S100B (inset 1). Apparently, S100B binding promotes conformational changes in this region and consequently leads to relative destabilization of the β-sheet in the V domain of RAGE, which is reflected in the increase of deuterium uptake. This result is in agreement with structural data obtained before, in which bound peptides are significantly distorted in the FL_RAGE-S100B complex as compared to corresponding fragments in exRAGE (Fig. 3C, D). Therefore, upon ligand binding, structural adjustments are not unexpected for both RAGE and S100B. Secondly, the opposite effect, i.e. increased protection, was most strongly pronounced in the TM domain (Fig. 7). Of note, the peptide of increased protection (GILGGLGTAALL) contains the well-characterized GxxxG consensus sequence, i.e. two glycines separated by any three amino acids, which is a common motif that enables interactions between TM helices of single-pass membrane proteins (Teese et al., 2015; Kleiger et al., 2002). This provides experimental confirmation of the TM helix arrangement assumed in the model. The observed protection upon S100B binding indicates stabilization of a region distal from the binding site and spatially separated by the flexible C1-C2 linker. Therefore, our results show a mechanism for allosteric signal transmission of the binding event across the structurally labile protein region to the membrane-embedded domain of the receptor. Subtle changes in HDX uptake, detected along the whole RAGE sequence indicate such small structural and/or dynamic adjustments. Likely, such structural stabilization of the transmembrane receptor helices upon ligand binding may reposition CT elements in such a way that recognition by downstream RAGE effectors becomes possible. Thus, the detected structural coupling of different regions of the receptor, which may be enhanced by its oligomerization, allows the binding signal to be transmitted efficiently across the membrane.

Molecular dynamics simulation

In order to assess stability and dynamical properties of the obtained model as well as to explore possible paths leading to the final RAGE tetramer with S100B tetramer assembly, a series of molecular dynamics (MD) simulations were conducted. The proposed model is stable in MD simulations at room temperature, with the most stable regions in TM and C2 domains. After 10ns MD run the RMSD between the initial (model) and final conformations of FL_RAGE without CT domain was 15.7Å and 5.1Å for simulation without and with S100B, respectively, which demonstrates

increased stability upon S100B binding (Fig. 8). The CT domain, despite being quite unstructured, also becomes more stable upon S100B binding with final RMSD drop from 11.3Å to 7.7Å to initial pose between S100B-free and S100B-binding RAGE (Fig. 8).

"57-65" and "70-79" peptides are stably bound by S100B. The assembly of RAGE and S100B tetramers was primarily guided by an observation that S100B domains accept one of the two RAGE fragments as described in the above sections (Fig. 3). MD simulations performed for RAGE monomers interacting with S100B confirmed that the interaction is indeed stable and may be used for guiding the overall assembly.

C1-C2 linker switches between open and closed conformation. The organization of RAGE molecules within the model of RAGE-S100B heterooctamer imposes substantial flexibility between VC1 modules which bind S100B tetramer and C2 domains underneath. The ten-amino acid long non-helical linker between C1 and C2 domain contains two prolines which introduce structural rigidity and isolation (Supplementary Fig. S1). The conjugated rotation around N–Cα (ϕ) and C–Cα (ψ) bonds between valine and two prolines switches between well pronounced "open" (Fig. 4. peripheral, light and dark green subunits) and "closed" (Fig. 4. central, orange and yellow subunits) linker conformations. Although the performed (up to several dozens of nanoseconds) MD runs were too short to capture the hinge-like movement involving the whole protein, more detailed and longer simulations for the linker alone demonstrated that the "open" ↔ "closed" fluctuations can be driven even by thermal fluctuations. The potential energy difference between those conformations (0.042 eV) is only ~1.7 times the energy of the thermal fluctuations of atoms at room temperature; therefore, the RAGE protein may fluctuate between the "open" and "closed" conformations if no other barriers emerge.

Both "open" and "closed" conformations distilled from MD simulations for the linker alone are stabilized within the full-length RAGE monomer (Supplementary Fig. S1 C and D). The "open" conformation may be stabilized by the glutamine (Gln264) and, to less extent, alanine (Ala263) moieties stemming from the adjacent β-sheet and forming a network of hydrogen bonds with two lateral glutamic acids of the linker. This hydrogen bond network is dissociated upon switching to the "closed" conformation, which conversely gets stabilized on the other side of the linker, where the arginine (Arg228) intercalates between two stems of the adjacent β-sheet. The arginine is then secured by a hydrophobic lid formed by the adjacent valine (Val229) and tryptophan (Trp230).

TM helices form a dimer of dimers. Since it has been shown before that the TM domain of RAGE is important for oligomerization (Moysa et al., 2019), we performed additional MD simulations of dimeric, trimeric and tetrameric complexes of the RAGE transmembrane helices (spanning residues 340–365). The helices move in pairs so that they may be conceived as a dimer of dimers rather than symmetric tetramer. More detailed quantum chemical calculations in modelled lipid bilayer confirmed that the very adjacent helices are able to preclude many nonspecific sidechain interactions and therefore build stable dimers. Two dimers expose complementary hydrophobic patches for non-covalent interactions which facilitates tetramer formation.

The modelled structure of the transmembrane helical tetrameric bundle remains stable in short (10ns) MD simulations in a lipid bilayer with the RMSD between the initial and final conformation of 1.7Å. The thermal fluctuations trigger only minor shifts between adjacent helices triggered by movements observed between the dimers which slide against each other. Zipper-like packing of the side chains within the dimers imposes an angle of about 20 degrees between their axes. Upon switching to the trimeric bundle (simply by removing one helix from the TM tetrad) the system evolved towards C3 symmetry. In order to reach an optimal sidechain packing a strong bend between the helices emerged which severely decreased the stability of such assembly. Taken together, these results suggest that the formation of RAGE tetramer, at least in its transmembrane part, occurs via assembling of two dimers, rather than grouping the monomers one by one.

Stoichiometry of RAGE oligomers. Native MS results (Fig. 1D) revealed the formation of dimers, trimers, and tetramers of RAGE. By subtracting monomers from the final model, we generated six different RAGE oligomeric assemblies, (Fig. 9) and subjected them to MD simulation in order to assess their dynamical behavior and stability.
Both simulated trimers (Fig. 9 3a and 3b) although stayed intact within the V, C1 and C2 domains eventually disassembled within TM helices which were unable to maintain a stable trimeric assembly as discussed above.

Two of the modelled dimers (Fig. 9 2a and 2c) were unstable within TM and C2 regions due to too big initial distances between the monomers (6–8 Å) which led to eventual dissociation of the subunits. In case of the dimer formed by two central RAGE monomers (Fig. 9 2c), the dissociation was not complete as the monomers remained stably connected in the C1 and V regions. Despite the artificiality of these two dimers naively distilled from the complete RAGE tetramer, this result demonstrates that interaction within TM elements is essential for maintaining stable dimerization. Two other dimers in which interact through TM and C2 domains (Fig. 9 2b and 2d) both remained stable in MD simulations despite VC1 modules being free to move.

Assuming high mobility of the VC1 modules relative to the C2 and TM domains the dimers should enable the Y-shaped conformation with both C1-C2 linkers in the "open" position which would increase flexibility and could eventually mitigate tetramer assembly. Both 2b and 2d dimers consist of one "open" and one "closed" subunit. While the 2d dimer would require opening both monomers prior to tetramerization, the 2b dimer might still be able to assemble into a tetramer without any major conformational changes. The 2b dimer is additionally stabilized by Asp73-Lys122 bonding between the V domain of the "closed" subunit and C1 domain of "open" subunit which renders it as even more probable intermediate in the assembly of eventual RAGE tetramer.

Discussion

Oligomerization is a common event used by multiple membrane-tethered receptors for signal transduction (Wu et al., 2013). RAGE receptor has been known for a long time to form oligomers and its oligomerization has been suggested in numerous studies as essential for the signal transduction mechanism (Yatime et al., 2013; Ostendorp et al., 2007; Xue et al., 2016; Koch et al., 2010; Zong et al., 2010). However, the structures of RAGE oligomers, either in free form or bound to S100B could not be determined due to substantial challenges in studying membrane complexes and intrinsic oligomerization tendencies of the extracellular part of RAGE itself. In this study, we approached this problem using the full-length RAGE construct, studied by native MS and cross-linking MS, combined with HDX-MS, 3D modelling and molecular dynamics simulations. We demonstrate that the interaction between the full-length RAGE and S100B occurs when both of them are in multimeric states. Based on the XL-MS data and available structures we modelled the complex of tetramer RAGE-tetramer S100B. Also, our HDX results indicated allosteric coupling of the distal extracellular V-domain, accepting S100B ligand, and the transmembrane region, which may be related to the way of signal transmission by RAGE oligomers into the cell. Eventually, based on MD results we speculate on the steps leading to the tetramer RAGE-tetramer S100B assembly formation.

Several models of RAGE-S100B complexes were proposed before (Fig. 10), all with a different arrangement of RAGE and S100B molecules. The parallel orientation of exRAGE in complexes was proposed by Ostendorp (Ostendorp et al., 2007) (Fig. 10A) and Koch (Koch et al., 2010) (Fig. 10B). Despite similarities in the organization of RAGE dimers in these two models, they differ in the way of how RAGE molecules interact with each other. Ostendrop's model (Fig. 10A) is based on the V-V interaction, while Koch argues that the interaction occurs mainly through C1 domains (Fig. 10B). Another variant of RAGE organization in the complexes with S100B was suggested by Xue (Xue et

al., 2016) (Fig. 10C). The model proposes stabilization of RAGE homo-dimer through the asymmetric interaction between V-C1 and C1-C2 domains.
The model developed in this study includes the CT domain and the transmembrane helices, with the latter one demonstrated to be important for oligomerization (Moysa et al., 2019). Furthermore, it assumes the interfaces between the different RAGE subunits to be more tightly packed. Eventually, studying the full-length RAGE reduces the possibility of considering incorrect oligomerization scenarios inferred from misleading interactions between truncated protein versions. Our model represents the full-length tetrameric RAGE in complex with tetrameric S100B with near-atomic resolution. Interestingly, the model and MD simulations propose the assembly of two dimers (see Fig. 10D yellow and light green or orange and dark green), each resembling immunoglobulins in their overall Y-shaped form when in "open" conformation. The interaction of these dimers through VC1 domains, interacting with S100B tetramer, is a central theme of the presented model.

An open question remains how RAGE oligomerization and S100B binding processes proceed in time. The stability of the central VC1 modules assembly (Fig. 9 2c) suggests that such dimer might constitute an oligomerization seed, which upon accepting S100B tetramer would recruit two additional, "peripheral" RAGE subunits. The central VC1 dimer buries considerable surface area and exposes extensive charged patch for S100B baiting. However, in order to maintain its stability, it would need to dimerize also within C2 and TM domains which are not immediately adjacent in our full tetrameric model. If the RAGE tetramer is indeed symmetrical in TM and C2 regions as we propose, these domains would need to reassemble upon binding of the incoming "peripheral" RAGE subunits. Also, in order to interact with S100B through both "57-65" peptides exposed from the "central" VC1 dimer, the "2c" variant of the RAGE dimer must bind to the full S100B tetramer. Conversely, the "2b" dimer (Fig. 9 2b) although not having such big buried area, can bind S100B dimer, a minimal functional S100B unit (Streicher et al., 2010), which would additionally stabilize it prior to binding another dimer S100B - dimer RAGE unit and forming the final tetrameric assembly. In contrast to tetramer, S100B dimer does not require Ca^{2+} ions to form so it might be also more abundant in the environment. Eventually, in the presence of Ca^{2+} S100B tetramer might form, promoting further steps of RAGE tetramerization. Binding of S100B dimer is even more likely since S100B stably binds to both "57-65" and "70-79" peptides lining the pocket formed by interacting V domain from the "closed" monomer and C1 domain from the "open" monomer. Also, the "2b" dimer maintains more stable, in the light of the proposed model, C2 and TM dimerization and requires no reassembly towards the formation of the final, symmetrical tetramer which additionally simplifies this scenario. Therefore, in our opinion, it is more likely that the formation of the RAGE tetramer starts with the "2b" dimer. And finally, we speculate that the full RAGE tetramer would assemble from two dimers without trimer formation.

RAGE oligomerization, required for signal transduction, is mediated by extracellular and transmembrane domains by imposing limitations on the arrangement of short, flexible CT tails. Restricting the space of possible conformations within the C-terminal region by allosteric changes dictated by the ligand type might effectively shape the arrangement of CT helices in a way suitable to bind particular effector molecules so that the ligand-specific intracellular response can be generated. Our results indicate the existence of only low order hetero-oligomeric complexes *in vitro* - from dimer RAGE - dimer S100B to tetramer RAGE - tetramer S100B, without strong preference to any one of them. Therefore, the minimal stoichiometry sufficient to reach the signalling threshold remains unknown and still needs to be determined.

The major common characteristics of known RAGE ligands are the net negative charge at physiological pH and the tendency for oligomerization (Fritz, 2011). For instance, the advanced glycation end products of proteins (AGEs) accumulate negative surface charge upon glycation (Bansode et al., 2020) and thus expose multiple sites for interaction with RAGE. Other RAGE ligands: S100 proteins (Pietzsch, 2011) and amyloid β peptide (Olubiyi et al., 2012) have also a net negative charge at physiological pH; so does the C-terminal domain of HMGB1 (Banerjee et al., 2003).

According to the presented model RAGE oligomerization results in the formation of a continuous, positively charged patch (Fig. 6B) baiting for such negatively charged ligands. Since RAGE interaction partners extensively differ in size and shape, the stoichiometry and shape of RAGE-ligand complexes may also be variable, depending on the ligand.

The molecular mechanism by which the information about the ligand-binding event is transferred in RAGE across the membrane from the V-domain, which is distal to the lipid bilayer, intrigued researchers for a long time. It has been argued that the very flexible linker between the C1 and C2 domain keeps them structurally uncoupled, and therefore disrupts the cascade of structural changes that might propagate across the RAGE monomer towards and through the membrane. The MD simulations in limited timescale accessible to modern computers were not enough to address this issue adequately. However, our HDX results proved otherwise since we have experimentally documented allosteric changes of structural stability in the TM region caused by distal binding of the ligand. The CT domain is linked to the transmembrane helix through a very short linker, and the juxtaposition of TM elements will undoubtedly affect the properties of the C-terminal RAGE region for binding potential intracellular ligands.

The involvement of RAGE in multiple pathological conditions makes it a critically important drug target. However, a variety of ligands can interact with different regions of the receptor, hampering the creation of one universal compound capable of modulating all aspects of RAGE activity. To overcome this issue, an alternative path was undertaken focusing on the much smaller effector CT domain and its inhibition instead (Manigrasso et al., 2016). Yet, with more data published, it appears that besides DIAPH1, RAGE may also bind other adaptor proteins, like ERK1/2, PKCζ, TIRAP, and DOCK7 (Ishihara et al., 2003; Sakaguchi et al., 2011; Yamamoto et al., 2013). Due to the limited size of the CT domain, it is much easier to disrupt its function, but concerning the unstructured nature of the C-terminal tail, it would be challenging to engineer more precisely targeted drugs. Therefore, searching for inhibitors of interactions between RAGE and one defined intracellular effector can be also unproductive. It is vital then to gain a detailed understanding of potential mechanisms through which RAGE interacts with its ligands in order to draw more general conclusions on RAGE function, eventually leading to more universal, rational inhibition strategies. Since the oligomerization is crucial for both ligand binding and signal transduction, a compound affecting the oligomerization pathway of RAGE might be such a universal inhibitor independent of the ligand's properties. Our model demonstrates several interaction interfaces between RAGE monomers, some of which might be crucial for the functionality of RAGE oligomers. Taking into account the emerging importance of RAGE in multiple diseases, further characterization of its complexes with other ligands is essential for rational and efficient drug design.

Figures

Figure 1. Native MS of S100B, FL_RAGE, and FL_RAGE-S100B. Spectra of S100B in the absence (A) and presence (B) of Ca show a homooligomerization of an even number of S100B subunits with tendencies of larger complex formation in the Ca-containing sample. (C) Increasing collision energies lead to the dissociation of S100B into monomers. (D) The oligomerization pattern of FL_RAGE ranges from monomers up to tetramers. (E) The complex formation of FL_RAGE-S100B (molar ratio 1:5) shows heterogeneous stoichiometries with a dimer (FL_RAGE)-dimer (S100B) and trimer (FL_RAGE)-dimer (S100B) as the most prevalent species. Oligomeric state and subunit stoichiometry of S100B, FL_RAGE, and FL_RAGE-S100B is annotated by red (FL_RAGE) and green (S100B) dots including the corresponding charge states.

Figure 2. XL-MS of RAGE and RAGE-S100B. (A) A cross-linking network of intramolecular links of FL_RAGE oligomers and FL_RAGE-S100B. Differences are highlighted in blue (observed only in free RAGE) and dark blue (observed only in RAGE-S100B complex). Green links were observed for both conditions. (B) A network of Intermolecular links of FL_RAGE oligomers and FL_RAGE-S100B. Differences are highlighted in purple (observed only in free RAGE) and red (observed only in RAGE-S100B complex). Green links were observed for both conditions. Intermolecular links observed between RAGE and S100B are shown in magenta. The visualization of a cross-linking network was made by xiNET - Cross-link viewer web server (Combe, et al., 2015).

Figure 3. S100B binds to the V domain of RAGE. (A) S100B dimer in complex with RAGE peptide 57-65 (pdb|4xyn) (B) S100B with RAGE 70-79 (pdb|5d7f); Reconstitution of RAGE-S100B interaction site by the superposition of corresponding RAGE fragments: (C) “57-65” and (D) “70-79”; (E) RAGE can be docked into a given binding site of S100B in two ways based on either “57-65” (yellow structure) or “70-79” peptide (green structure) (F) superposition of pdb|4xyn and pdb|2h61 structures show how S100B dimer might interact with different RAGE fragments (G) assembly of S100B tetramer with RAGE fragments based on the 3D structure of S100B octamer (pdb|2h61).

Figure 4. 3D model of FL_RAGE and its complex with S100B. RAGE chains marked yellow contact S100B tetramer via “57-65” region placed in “central” binding sites while marked green via “70-79” region placed in “peripheral” sites. Insets detail the V, C1 and C2 domains at intermolecular contact regions. The generic lipid bilayer was generated using Charmm-Gui Membrane Builder (Lee et al., 2019).

Figure 5. Intra- and intermolecular cross-links overlaid on the 3D model of the complex. (A) Intramolecular links within RAGE V-C1 domains. (B) Cross-links between S100B tetramer and four RAGE VC1 units. (C) Intermolecular cross-links between RAGE subunits. Differences are highlighted in purple and blue (observed only in free RAGE), and red and dark blue (observed only in RAGE-S100B complex), purple and red indicating intermolecular links while blue and dark blue intramolecular. Green links were observed for both conditions. Intermolecular links between RAGE and S100B are shown in magenta. Only cross-links satisfying the 30 Å distances limit are shown.

Figure 6. Electrostatic interaction upon complex formation. (A) C1 domain presents negatively charged patches favouring interactions with the positively charged V domain. One RAGE subunit was depicted as a molecular surface and coloured according to electrostatics while the other molecule is presented as an outline to illustrate the binding cleft. (B) V-domains in RAGE dimer form a continuous single positively charged patch, a plausible interface to interact with the negatively charged surface of the S100B tetramer. Red negative, blue - positive charge.

Figure 7. HDX-MS analysis of FL_RAGE. The differential plot shows differences in deuterium uptake measured on the peptide level for both FL_RAGE and FL_RAGE-S100B (see details in the material and methods). The blue and red area indicates increased and decreased protection upon ligand binding, respectively. Deprotection (red) and protection (blue) of peptides is superimposed on the model structure and largest differences are highlighted by rectangles.

Figure 8. Dynamical evolution of modelled FL_RAGE structure in MD simulation. RMS distance is calculated for protein backbone between conformation at the given trajectory point and the starting point. The RMSD values were derived from the same trajectory independently for the C-terminal domain (left panel) and the rest of FL_RAGE (right panel).

Figure 9. RAGE oligomers used for MD simulations.

Figure 10. Schematic comparison of RAGE models published to date. (A) Ostendorp's model assumes a fully parallel orientation of RAGE molecules with special emphasis on tightly formed V-V dimer interaction when interacting with S100B. (B) Koch's model also follows the idea of mostly parallel RAGE orientation, yet with interactions mainly maintained through C1 domains. (C) Xue's model proposes a dimerization via V-C1 and C1-C2 interactions upon S100B binding. (D) Heterooctamer model reported in this paper. Dashed rectangles outline the domains of RAGE which have been considered in each study.

STAR★Methods

Key Resources Table

REAGENT or RESOURCE	SOURCE	IDENTIFIER
Bacterial and Virus Strains		
DH5α (Single shot - Max efficiency)	Invitrogen by Thermo Fisher Scientific	Cat#44-0097
BL21(DE3)	NEB	Cat#C2527I
Chemicals, Peptides, and Recombinant Proteins		
Luria Bertani Broth	Sigma	Cat#L3022
LB Agar (Lennox)	Sigma	Cat#L2897
Kanamycin Sulfate	Thermo Fisher Scientific	Cat#11815032
IPTG	Sigma	Cat#I6758
Glycerol	Penta	Cat#14550-11000
DNase	Roche	Cat#4716728001
cOmplete™ EDTA-free protease inhibitor	Roche	Cat#04693132001
Tris hydrochloride	Sigma	Cat#10812846001
NaCl	Sigma	Cat# S3014
EDTA	Sigma	Cat#E9884
TCEP	Sigma	Cat#C4706
DTT	GE Healthcare	Cat# GE17-1318-02
HEPES	Sigma	Cat#H3375
Imidazole	Sigma	Cat#56749
Triton™ X-100	Sigma	Cat#11332481001
Ammonium chloride (15N, 99%)	Cambridge isotope laboratories	Cat#NLM-467-PK
BS3 (bis(sulfosuccinimidyl)suberate)	Thermo Fisher Scientific	Cat#A39266
Sequencing Grade Modified Trypsin	Promega	Cat#V5111
Deuterium oxide	Cambridge isotope laboratories	Cat#DLM-4-PK
GdnHCl	Sigma	Cat#G3272-100G
Chymotrypsin, Sequencing Grade	Promega	Cat#V1061
Endoproteinase Glu-C from Staphylococcus aureus V8	Sigma	Cat#P6181-50UG
Deposited Data		
X-ray structure RAGE extracellular domains	(Yatime et al., 2016)	PDB: 4ybh
Interaction of S100B with a peptide derived from the RAGE V domain	(Jensen et al., 2015)	BMRB: 4xyn
Interaction of S100B with a peptide derived from the RAGE V domain	N/A	PDB: 5d7f

NMR structure of RAGE C-terminal domain (CT)	(Rai et al., 2012)	PDB: 2lmb
X-ray structure of human Ca2+-loaded S100B	(Ostendorp et al., 2007)	PDB: 2h61
Model of RAGE-S100B heteroocatamer	This paper	PDBDEV: 00000080
RAW data of XL-MS of RAGE oligomeric complexes.	This paper	MSV000086438
RAW data of XL-MS of RAGE-100B complex.	This paper	MSV000086437
RAW data of HDX-MS experiment	This paper	MSV000086718
Oligonucleotides		
FL_RAGE forward primer. 5'-CTGATCATATGAAAAAAACCGCGATTGCGATTGCGGTGGCGTTAGCG GGCTTTGCGACCGTGGCGCAGGCGGGCGCGCAAAACATTACCGCG-3'	This paper	N/A
FL_RAGE revers primer. 5'-CTGATCTCGAGCGGGCCGCCGGTGCT-3'	This paper	N/A
Recombinant DNA		
pET24a FL_RAGE	This paper	Genscript
pAED4 S100B	This paper	N/A
Software and Algorithms		
PyMOL	DeLano Scientific LLC	http://www.pymol.org/
xiNET	Combe, et al., 2015	http://crosslinkviewer.org/
ESIprot Online	Winkler et al., 2010	https://www.bioprocess.org/esiprot/esiprot_form.php
UniDec	Marty et al., 2015	https://github.com/michaelmarty/UniDec/releases
MeroX2.0	Götze et al., 2014	http://www.stavrox.com/
HaDex	Puchała et al., 2020	https://hadex.mslab-ibb.pl/
SPDBV	Guex et al., 1997	https://spdbv.vital-it.ch/
Rosetta	Andre et al., 2007	https://www.rosettacommons.org/software
CoCoMaps	Vangone et al., 2011	https://www.molnac.unisa.it/BioTools/cocomaps/
GROMACS 2019.4	Berendsen et al., 1995	https://www.gromacs.org/
CHARMM-GUI	Lee et al., 2019	http://www.charmm-gui.org/
Other		
Poroszyme™ Immobilized Pepsin Cartridge	Applied Biosystems	Cat# 2313100
Mini-PROTEAN® TGX™ Precast Protein Gels	Bio-Rad	Cat#4561094
Ni-NTA	Sigma	Cat#P6611-100mL
Superdex 200 10/300 GL	GE Healthcare	Cat#GE17-5175-01
HiTrap SP HP column	GE Healthcar	Cat#GE17115101

	e	
Amicon Ultra-4 Centrifugal Filter unit 100kDa cutoff	Millipore	Cat#UFC810024
Amicon Ultra-15 Centrifugal Filter unit 10kDa cutoff	Millipore	Cat#UCF901024

Table S1. Cross-linked peptides identified for RAGE and S100B proteins, Related to Figures 2, 5

Table S2. Percentage of peptide deuteration analysed in HDX-MS experiment, Related to Figure 7

Model structure. 3D structure of RAGE-S100B complex discussed in this study, Related to Figures 4, 5, 9

Resource Availability

Lead Contact

Further information and requests for reagents and resources may be directed to, and will be fulfilled by the Lead Contact Alexander Moysa (a.alexandrmoysa@gmail.com)

Material Availability

This study did not generate any new unique reagents. All plasmids used in this study are available upon request.

Data and Code Availability

No novel code was generated during this work. Atomic coordinates and structure factors for the model have been deposited to the PDB-Dev repository (accession number is PDBDEV_00000080). Raw files corresponding to the XL-MS as well as HDX-MS analysis of the RAGE and RAGE-S100B samples have been deposited to the MassIVE repository with the dataset identifiers MassIVE MSV000086438, MSV000086437, MSV000086718.

Experimental Model and Subject Details

Recombinant proteins were expressed using *E.coli* strain BL21(DE3) (NEB) Further specific information are specified in Method Details

Method Details

Protein expression and purification

FL_RAGE and S100B proteins were overexpressed in *E.coli* as described previously (Moysa et al., 2019; Zhukova et al., 2004). Codon optimization and gene synthesis of FL_RAGE was performed by the GenScript. The FL_RAGE genes were cloned into the *E. coli* expression vector pET24 thus to provide the expressed proteins with C terminal histidine tag. The FL_RAGE genes, covering amino acid positions 22 to 404, respectively, were amplified by polymerase chain reaction (PCR) using the primers of the sequences provided in the Key resources table. To maintain nativelike redox conditions, instead of cytoplasmic E. coli expression of FL_RAGE, we used a periplasmic expression system that allowed acquisition of correct pairing of disulphide bonds and avoidance of disulphide-mediated aggregate formation, as can be observed for cytosolic expression systems (see details in Moysa et al., 2019) Therefore, the forward primer contained a sequence of the signal peptide of OmpA *E. coli*. The N-terminal primer the contained *NdeI* restriction site, and the C-terminal

oligonucleotides coded for the *XhoI* restriction site. PCR was performed using Pfu DNA polymerase (Thermo Fisher Scientific) following the manufacturer's protocol. The resulting PCR fragments were digested with *NdeI* and *XhoI* (Thermo Fisher Scientific). The fragments were ligated to a pET24 vector using T4 DNA ligase (Thermo Fisher Scientific) and the recombinant clones sequenced to confirm the inserts. Plasmids were transformed into the E. coli strain BL21(DE3) for expression. Frozen bacterial stocks were maintained at −80°C in LB medium containing 50 µg/ml kanamycin and 15% glycerol. For the overexpression, a frozen glycerol stock of BL21(DE3) cells transformed with plasmid-encoding protein was streaked onto an LB agar plate containing 50 µg/ml kanamycin and grown overnight at 37°C. The resultant bacterial colonies were resuspended in 50 ml of LB Broth medium (Formedium) containing 50 µg/ml kanamycin and grown at 37°C with shaking at 160 rpm for 4 hours. A total of 16 ml of bacteria was used to inoculate 1 l of LB Broth medium containing 50 µg/ml kanamycin in 5-l Erlenmeyer flasks. The culture was grown at 37°C with shaking at 160 rpm until OD600 reached 0.7–0.8 and induced by adding Isopropyl β-D-1-thiogalactopyranoside to a final concentration of 1 mM. The culture then was incubated overnight at 160 rpm and 25°C. Bacteria were harvested by centrifugation at 5000 ×g in a centrifuge (Beckman Counter, Fullerton, CA, USA). The medium was removed, and the cells resuspended in 100 ml buffer (0.05 M Tris–HCl, 0.3 M NaCl, and 1 mM PMSF, pH 8.0) per 4 l of culture. For solubilization of protein 2% of Triton X-100 was used. The lysozyme treatment was carried out with 10 mg/ml of lysozyme for 30 minutes on ice. The sonication was done for 5 minutes while incubating on ice, using the manufacturer's protocol. After sonication for better solubilization samples were gently mixed overnight at 4°C before centrifugation. The extracts were clarified by centrifugation for 30 minutes at 14,000 rpm at 4°C. Extracts after centrifugation were then mixed with 2 ml of Ni Sepharose 6 Fast Flow slurry (GE Healthcare), pre-equilibrated with lysis buffer. Samples were incubated with Ni Sepharose slurry at 4°C on a shaker at low speed overnight. The Ni Sepharose was washed with 10 column volumes of lysis buffer and 10 column volumes of wash buffer (50 mM Tris–Cl, 1 M NaCl, 50 mM imidazole, pH 8.0 Triton X-100 0.04% (w/v) (2 CMC)). Protein was eluted with buffer (50 mM Tris–Cl, 0.5 M NaCl, 250 mM Imidazole, pH 8.0 and Triton X-100 0.04% (w/v)). The next stage of FL_RAGE purification was carried out using HiTrap SP cation exchange column (GE Healthcare) at pH 7.4 (50 mM TrisHCl, 0.2 M NaCl and 0.04% (w/v) of Triton, a salt gradient from 0.2 M to 1 M NaCl. Fractions containing pure protein were combined and concentrated using an Amicon Ultra Centrifugal Filter Unit 100K WMCO to ~5 mg/ml and stored at 4°C. For the expression of 15N FL_RAGE, instead of LB Broth medium the Minimal growth medium with $H_4Cl^{15}N$ was used according to the protocol: https://www.helmholtz-muenchen.de/fileadmin/PEPF/Protocols/M9-medium_150510.pdf.

S100B was expressed in *E. coli* (HMS174(DE3) strain) using pAED4 based expression plasmid. IPTG (0.4 mM) was used to induce protein expression for 2 h at 36 °C. Cells were harvested by centrifugation at 5000g for 10 min. For protein purification, 15 g of cells were typically suspended in 30 ml 50 mM Tris–HCl, 5 mM $MgCl_2$ pH 7.6 and sonicated for 5 minutes on ice. After cell breakage, 0.5 mM PMSF was added, and the crude extract was centrifuged at 14,000 rpm for 30 minutes. The supernatant was diluted with 50 mM Tris–HCl pH 7.6 and 2 mM $CaCl_2$ was added. The diluted supernatant was then loaded onto a phenyl-Sepharose column (100 ml volume; Amersham, GE-Healthcare) equilibrated with 50 mM Tris–HCl, 2 mM $CaCl_2$ pH 7.6. The column was washed with 20 volumes of the same buffer and bound S100B protein was eluted with 50 mM Tris–HCl, 5 mM EDTA pH 7.6.

Nucleotide sequence of FL_RAGE in the plasmid

GCGCAAAACA TTACCGCGCG TATCGGCGAG CCGCTGGTGC TGAAGTGCAA AGGTGCGCCG AAGAAACCGC CGCAGCGTCT GGAGTGGAAG
CTGAACACCG GCCGTACCGA AGCGTGGAAA GTTCTGAGCC CGCAAGGTGG CGGTCCGTGG GACAGCGTGG CGCGTGTTCT GCCGAACGGT
AGCCTGTTCC TGCCGGCGGT TGGCATCCAG GATGAGGGTA TTTTTCGTTG CCAAGCGATG AACCGTAACG GCAAGGAAAC CAAAAGCAAC
TACCGTGTGC GTGTTTATCA GATCCCGGGC AAGCCGGAAA TTGTTGATAG CGCGAGCGAG CTGACCGCGG GCGTGCCGAA CAAAGTTGGT
ACCTGCGTGA GCGAAGGCAG CTATCCGGCG GGTACCCTGA GCTGGCACCT GGACGGCAAG CCGCTGGTGC CGAACGAAAA GGGTGTGAGC
GTTAAAGAGC AGACCCGTCG TCACCCGGAA ACCGGTCTGT TCACCCTGCA AAGCGAACTG ATGGTTACCC CGGCGCGTGG CGGTGACCCG
CGTCCGACCT TCAGCTGCAG CTTTAGCCCG GGTCTGCCGC GTCATCGTGC GCTGCGTACC GCGCCGATTC AACCGCGTGT TTGGGAGCCG
GTGCCGCTGG AGGAAGTGCA ACTGGTGGTT GAGCCGGAGG GCGGTGCGGT TGCGCCGGGC GGTACCGTGA CCCTGACCTG CGAAGTTCCG
GCGCAGCCGA GCCCGCAAAT TCACTGGATG AAGGATGGTG TGCCGCTGCC GCTGCCGCCG AGCCCGGTTC TGATCCTGCC GGAGATTGGC
CCGCAGGATC AAGGTACCTA TAGCTGCGTG GCGACCCACA GCAGCCATGG TCCGCAGGAG AGCCGTGCGG TTAGCATCAG CATCATTGAA
CCGGGTGAGG AAGGTCCGAC CGCGGGTAGC GTGGGCGGTA GCGGCCTGGG TACCCTGGCG CTGGCGCTGG GCATTCTGGG CGGTCTGGGT
ACCGCGGCGC TGCTGATCGG CGTTATTCTG TGGCAGCGTC GTCAACGTCG TGGTGAGGAA CGTAAAGCGC CGGAAAACCA AGAGGAAGAG
GAAGAGCGTG CGGAACTGAA CCAAAGCGAA GAACCGGAGG CGGGCGAAAG CAGCACCGGC GGCCCG

Native MS

Samples were desalted and buffer-exchanged using P-6 Micro Bio-Spin columns (Bio-Rad) pre-equilibrated with an MS-compatible solution which varied depending on the protein system. The solution applied for the different proteins were as follows: 100 mM NH_4OAc with or without 0.2 mM $CaCl_2$ for S100B; 300 mM NH_4OAc, 0.04% Triton X-100 for FL_RAGE; and 300 mM NH_4OAc, 0.04% Triton X-100, 0.05 mM $CaCl_2$ for the FL_RAGE-S100B complex. The protein concentration was 20 µM for both FL_RAGE and S100B and a molar ratio of 1:5 was used between FL_RAGE (~10 µM) and S100B (~50 µM) for FL_RAGE-S100B complex formation. MS experiments were conducted either on a Synapt G2 HDMS (Q-ToF instrument; Waters) or a Q Exactive UHMR (hybrid quadrupole-orbitrap instrument; Thermo Fisher Scientific) mass spectrometer. For this purpose, samples were loaded into in-house produced gold-coated borosilicate glass capillaries and introduced into the mass spectrometer by nano-electrospray ionization using positive ion mode. MS measurements of S100B were conducted under the following major settings for optimal ion transmission on the Synapt G2 HDMS instrument: TOF mode, 1.6kV capillary voltage, 25V sampling cone, 5V extractor cone, 5mbar backing pressure, 30°C source temperature, and 5V collision energy in the trap and transfer collision cell filled with argon at $3.0x10^{-2}$ mbar pressure.

MS measurements of FL_RAGE and the FL_RAGE-S100B complex were conducted on a Q Exactive UMHR mass spectrometer. To that end, collision energies in the instrument were tuned for gentle release of the micelle-embedded membrane protein complex with the following main settings: 1.6 kV capillary voltage, 250 V (200 V for FL_RAGE) in-source trapping, and 50 V in-source CID. The RF applied throughout the instrument were set to 700 Vp-p, 940 Vp-p, and 2950 Vp-p for the injection flatapole, bent flatapole, and the C-trap, respectively. The transmission of ions was optimized by a voltage gradient in the ion transfer optics which was set to 5, 4, 2, 0 V for the injection flatapole, inter flatapole, bent flatapole, and transfer multipole, respectively (Gault et al., 2016).

XL-MS

Preparation of cross-linked protein complexes

To distinguish between intra- and intermolecular cross-links of RAGE, we prepared a mixture of unlabeled and isotopically 15N-labeled FL_RAGE. Both unlabeled and isotopically labeled FL_RAGE were mixed at a molar ratio of 1:1 and incubated overnight at 4°C. The ratio of unlabeled to isotopically labeled FL_RAGE was evaluated by LC-MS (Supplementary Fig. S2). Complexes of FL_RAGE-S100B were prepared in a 1:5 molar ratio using 20 mM HEPES pH 7.4, 200 mM NaCl, 3 mM $CaCl_2$, 0.04% Triton X-100. The mixture was incubated for 1h before being cross-linked by addition of BS3 to a final molar ratio of 50:1 BS3/protein for 2h on ice. The reaction was quenched by adding excess (50 mM) ammonium bicarbonate, and the quenched solution was further incubated at room temperature for 1h. Protein complexes were concentrated using a 100K MWCO spin column and applied to size exclusion chromatography using a Superdex 200 10/300 GL (GE Healthcare) column equilibrated with 25 mM Tris-HCl, 0.3 M NaCl, pH 7.4; 0.04% (w/v) of Triton. Samples were collected in 0.25-ml fractions which were subsequently evaluated by SDS-PAGE (Supplementary Fig. S3). Samples were mixed with a 2x sample buffer containing 200 mM DTT, boiled at 80°C for 10 minutes, and were loaded on a discontinuous gel system with 4–15% Mini-PROTEAN® TGX™ Precast Protein Gels Bio-Rad. Unstained Protein Molecular Weight Marker (Thermo Fisher Scientific) was used. Electrophoresis was conducted with a Bio-Rad mini protean tetra cell gel system under a continuous voltage of 100 V. Protein bands were visualized by silver staining(Chevallet, Luche, and Rabilloud 2006).

Digestion and sample preparation for mass spectrometry analysis

Selected SEC fractions (Supplementary Fig. S3) were subjected to sequential digestion, in which different proteases are applied to reduce the size of large tryptic peptides allowing access to sequence space that would otherwise remain undetected (Mendes et al., 2019). SEC fractions were concentrated to ~30 ul using Microcon-10kDa centrifugal filter units. Further steps were performed in

accordance with Filter Aided Sample Preparation (FASP) method (Ni et al., 2017). Protein samples (~20 µg) were mixed with 200 µl of 8 M urea in 0.1 M Tris–HCl (pH 8.5) 0.05 M TCEP and after 30 minutes incubation at room temperature were transferred onto a filter device which were centrifuged at 14,000 g at 20°C for 15 min. All further buffer exchanges were performed by centrifugation under identical conditions. The concentrate was diluted with 200 µl of 8 M urea in 0.1 M Tris–HCl (pH 8.5) and 0.05 M iodoacetamide. Then the mixture was incubated for 20 min in the dark prior to centrifugation. The resulting concentrate was diluted with 100 µl of 8 M urea in 0.1 M Tris–HCl (pH 8.5) and was centrifuged again. This step was repeated twice. The concentrate was then diluted with 100 µl of 50 mM ammonium bicarbonate and centrifuged again. This step was performed twice. The concentrate was then subjected to trypsin digestion. Trypsin was added at an enzyme-to-substrate mass ratio of 1:50, and samples were incubated overnight at 37°C. The reaction was stopped by adding 10% (v/v) TFA, and samples were divided into three parts and were desalted using C18-StageTips and further lyophilized. Tryptic peptides were resuspended in 100 ul of 50 mM ammonium bicarbonate and digestion was continued with a final protease: protein ratio using (1) GluC 1:50 (w/w), (2) chymotrypsin 1:50 (w/w), and (3) trypsin 1:100 (w/w). Samples were incubated overnight at 37°C. The reaction was stopped by adding 10% (v/v) TFA and the sample volume was reduced to 50 µl by evaporation using a vacuum concentrator.

LC-MS/MS

Samples were analyzed using a Nano-Acquity LC system (Waters) coupled to a Q Exactive mass spectrometer (Thermo Scientific). The peptide mixture was applied to an RP-18 trap (nanoACQUITY Symmetry® C18 – Waters) using 0.1% trifluoroacetic acid (v/v) in water as a mobile phase. Peptides were then transferred to a nano-HPLC RP-18 column (nanoACQUITY BEH C18 - Waters 186003545) using an acetonitrile gradient (0–60% acetonitrile in 180 min) in presence of 0.05% formic acid and a flow rate of 250 nl/min. The column outlet was coupled directly to the ion source of the Q Exactive mass spectrometer working in the regime of data-dependent acquisition mode. Full-scan spectra were acquired in the mass range of m/z 300–2000 and a resolution of R = 120000. Up to 10 HCD MS/MS scans were performed on the most intense precursor ions with charge states between 3 and 8 using the following settings: resolution 30000, isolation window 4.0 m/z, stepped collision energy 40.0, dynamic exclusion 20.0 s.

XL-MS data analysis

Thermo raw data files were processed using MeroX2.0. For the cross-linked peptide search, the parameters used were as follows: MS accuracy, 10 ppm; MS/MS accuracy, 20 ppm; enzyme, trypsin, trypsin + chymotrypsin or trypsin + GluC depending on the sample digestion conditions; missed cleavages allowed, 4. Cysteine carbamidomethylation and methionine oxidation were set as fixed and variable modifications, respectively. The dead-end reaction was set as hydrolyzed cross-linker and amidated cross-linker. Reaction specificity for BS3 was considered for Lysine, Serine, Threonine, Tyrosine and the protein N-terminus. MS/MS spectra of identified cross-linked peptides were manually inspected.. Differentiation between intra- and intermolecular links was performed based on manual inspection of precursor MS spectra of the sample containing both labeled and unlabeled FL_RAGE (~1:1 molar ratio). Precursors of “mixed” cross-linked peptides (light/heavy and heavy/light) indicate the presence of intermolecular cross-links, whereas “pure” light and heavy cross-linked peptides are representative for intramolecular links (Supplementary Fig. S4).

HDX-MS

Prior to HDX, both FL_RAGE and FL_RAGE-S100B (1:5 molar ratio) (20 µM in 20 mM HEPES (pH 7.4), 200 mM NaCl, 3 mM $CaCl_2$, 0.04% Triton X-100) were equilibrated to 25 °C. HDX was initiated by 10-fold dilution (90% D2O) of the equilibrated sample with deuterated labelling buffer (20 mM HEPES, pH=7.4, 200 mM NaCl, 3 mM $CaCl_2$, 0.04% Triton X-100 in D2O) and incubated at 25°C for selected time points (1 min, 30 min and 24 h). The labelling reaction (50µ l) was quenched by adding ice-cold quench buffer (2 M glycine buffer, (pH=2.3), 4 M GdnHCl, and 0.5M TCEP) in a 2:1

ratio. Quenched samples were immediately frozen in liquid nitrogen and stored at −80 °C until analysis by LC-MS. Two control experiments were performed considering both in-exchange and out-exchange artefacts. Briefly, to assess minimum exchange (in-exchange control), a deuterated buffer was added to the ice-cold quench solution prior addition of the protein sample and flash freezing in liquid nitrogen as described above. The out-exchange (maximally labeled) control sample was prepared by 10-fold dilution with deuterated buffer (20 mM HEPES, pH=7.4, 200 mM NaCl, 3 mM $CaCl_2$, 0.04% Triton X-100 in D_2O) and incubated for 24 h at 4 °C before quenched and flash-frozen in liquid nitrogen.

Labeled samples were quickly thawed and injected onto a refrigerated (0 °C) UPLC station (NanoAcquity, Waters) with a 50 µl sample loop. The samples were passed through the immobilized pepsin cartridge (Applied Biosystems Poroszyme) at a flow rate of 150 µl/min using 0.23% formic acid in MQ water as mobile phase A. Generated peptides were trapped on a C18 Vanguard column (C18, 130 Å, 1.7 µm, 2.1 mm × 5 mm; Waters) and desalted for 2.5 min at a flow rate of 150 µl/min. Desalted peptides were separated on an Acquity Peptide BEH C18 UPLC column (130 Å, 1.7 µm, 2.1 mm × 50 mm; Waters), applying a linear gradient from 5% to 50% mobile phase B (0.23% formic acid in ACN) over 7 min. Separated peptides were eluted into a Synapt G2 mass spectrometer (Waters). Crucial parameters were set as follows: ESI positive mode, capillary voltage 3 kV, sampling cone voltage 40 V, extraction cone voltage 4 V, source temperature 80°C, desolvation temperature 175°C, and desolvation gas flow 600 L/h. Spectra were acquired in m/z range between 50 – 2000 m/z and MS^E mode with CID ramp 20-45 V for peptides identification and IM-MS mode (constant wave height of 40 V, wave velocity of 600 m/s) for obtaining of peptides deuterium uptake values. Peptides were identified using ProteinLynx Global Server software (Waters) using a control (undeuterated) FL_RAGE sample processed in the same manner. Three technical replicates were acquired for both protein states and each labelling time point.

The list of identified peptides is presented in the supplementary data (Supplementary Table S2). Identified peptides were analyzed by DynamX 3.0 (Waters) applying the following acceptance criteria: minimum intensity threshold of 3000, minimum products per amino acid of 0.2, RT deviation ± 10 s, and m/z deviation ± 10 ppm. Isotopic envelopes of deuterium-labeled peptides were analyzed in DynamX 3.0 with manual corrections wherever necessary. Percentage of peptide deuteration was calculated using HaDeX tool (Puchała et al., 2020), which takes the molecular weights of minimum (M_{ex}^0) and maximum exchange (M_{ex}^{100}) values of a given peptide into account.

$$\mathrm{D}\ (\%) = \frac{M_{ex} - M_{ex}^0}{M_{ex}^{100} - M_{ex}^0} \cdot 100\%$$

To calculate the overall degree of protection of a given peptide (aggregated protection, shown in Fig.8), we used kinetic plots showing the fraction of deuterium exchange at different labelling times points. These plots monitor the increase in deuteration in each peptide over time. The exchange in fully accessible regions occurs instantaneously, and the kinetic curve, linking the data points at different labelling times (1 min, 30 min and 24 h), is flat at 100% of exchange. Conversely, the kinetic curve of fully protected regions shows 0% exchange over the time course of the experiment. To characterize the overall protection by a single number, we calculated the area under the kinetic curve, obtaining a degree of protection in % (aggregated protection), usually a number between 0% of protection in fully flexible regions and 100% of protection of fully protected, non-exchanging regions. Based on these numbers, the differential aggregated protection (ΔHD_{ex}) was calculated by subtraction of the aggregated protection in common peptides of FL_RAGE and FL_RAGE-S100B. Final graphs were plotted using OriginLab 9.

3D modelling

The model of interaction between VC1 RAGE fragment and S100B was assembled manually using known structures of RAGE and S100B using SPDBV (Guex et al., 1997). C2 and TM tetramers were modelled separately using Rosetta symmetrical dock protocol (Andre et al., 2007). CT structure was predicted using fold and dock protocol in Rosetta (Dasa et al., 2009). The domains were connected with loops built with Rosetta's remodel (Huang et al., 2011). The model was relaxed with Rosetta relax (Nivón et al., 2013; Conway et al., 2014) and backrub (Smith et al., 2008) protocols. Lipid bilayer was built by Charmm-Gui Membrane Builder (Lee et al., 2019) in accordance with recommended parameters. Structures were visualized with Pymol (Schrodinger LLC 2015). Electrostatic potentials were computed and visualized using the APBS plugin in Pymol. Surface accessible areas were calculated using CoCoMaps tool (Vangone et al., 2011).

Molecular Dynamics simulations

In order to gain more insight into the receptor-ligand interactions of the RAGE-S100B complex, a series of molecular dynamics simulations in an environment mimicking physiological solution has been performed. The proposed model and its various fragments have been used as the base for starting configurations for calculations focused on finding the role of each protein fragment in the processes of the receptor's assembly and ligand binding. The energy analysis of the investigated systems allowed to quantify the interactions and stability of the proposed RAGE model alone and upon its interaction with S100B ligand. The simulations of the molecular mechanics and dynamic behavior of the RAGE receptor model alone complexed with S100B as well as their alleged intermediates have been carried out using GROMACS 2019.4 simulation package (Berendsen et al., 1995), with AMBER99SB-ILDN force field (Lindorff-Larsen et al., 2010) specially designed for the study of biological systems, with a total simulation time of ~10 ns each. Additionally, the TM fragments extracted from the proposed full-length RAGE model has been simulated with lipid bilayer using CHARMM26 force field, dedicated to simulating membrane-protein systems (Huang et al., 2013). Such TM fragments representing the main conformational states obtained from the full-length RAGE simulations (obtained from the principal component analysis, PCA) on the basis of MD trajectory have been verified by density functional theory (DFT). In order to properly describe the non-bonding interactions between the helices, the DFT geometry optimizations of the TM oligomers of different sizes (from dimer to tetramer) have been calculated using the CAM-B3LYP hybrid functional with 6-31G(d) Pople's basis set. To consider the surrounding of the helical bundle, the effect of the lipid bilayer with the polarized continuum method (PCM) has been used as implemented in Gaussian09 program package (Frisch, 2009).

Quantification and Statistical Analysis

The percentage of peptide deuteration was calculated using HaDeX tool using equation described in the method details, and the data reported in the Table S2. The standard deviations for the percentage of peptide deuteration were calculated by Excel.

Acknowledgements

We acknowledge financial support from EU infrastructural projects CEPT (POIG.02.02.00-14-024/08-00) and Foundation of Polish Science TEAM TECH CORE FACILITY/2016- 2/2 Mass Spectrometry of Biopharmaceuticals - improved methodologies for qualitative, quantitative and structural characterization of drugs, proteinaceous drug targets and diagnostic molecules. The equipment used in this study was sponsored by the National Multidisciplinary Laboratory of Functional Nanomaterials (POIGT.02.02.00-00-025/09-00). This work was supported by the National Science Centre, Poland: MAESTRO grant (2014/14/A/NZ1/00306) to M.D. and A.M. and POL-OPENSCREEN Grant #

DIR/WK/2018/06 from the Ministry of Science and Higher Education to K.S and OPUS Grant # 2018/31/B/ST4/03809 to D.N. The Antwerp University Research Fund for the Concerted Research Actions grant (BOF-GOA 4D protein structure) to D.H. The Q Exactive UHMR instrument was funded by the Wellcome Trust multi-user equipment grant 208385/Z/17/Z. This research was supported in part by PLGrid Infrastructure.

Author Contributions

Conceptualization, A.M., K.S., D.N., and M.D.
Methodology, K.S., D.N., A.M.
Investigation, A.M., K.S., D.N., D.H., L.Z.
Resources, F.S. and M.D.
Writing – Original Draft, A.M., K.S., D.H., D.N.
Writing – Review & Editing, A.M., K.S., D.N., F.S., and M.D.
Visualization, K.S.
Funding Acquisition and Supervision, M.D.

Declaration of Interests

The authors declare no competing interests

REFERENCES

Andre, Ingemar, Philip Bradley, Chu Wang, and David Baker. 2007. “Prediction of the Structure of Symmetrical Protein Assemblies.” *Proceedings of the National Academy of Sciences of the United States of America* 104 (45): 17656–61. https://doi.org/10.1073/pnas.0702626104.

Banerjee, Sourav, and Tapas K. Kundu. 2003. “The Acidic C-Terminal Domain and A-Box of HMGB-1 Regulates P53-Mediated Transcription.” *Nucleic Acids Research* 31 (12): 3236–47. https://doi.org/10.1093/nar/gkg412.

Bansode, Sneha, Uliana Bashtanova, Rui Li, Jonathan Clark, Karin H. Müller, Anna Puszkarska, Ieva Goldberga, et al. 2020. “Glycation Changes Molecular Organization and Charge Distribution in Type I Collagen Fibrils.” *Scientific Reports* 10 (1). https://doi.org/10.1038/s41598-020-60250-9.

Berendsen, H. J.C., D. van der Spoel, and R. van Drunen. 1995. “GROMACS: A Message-Passing Parallel Molecular Dynamics Implementation.” *Computer Physics Communications* 91 (1–3): 43–56. https://doi.org/10.1016/0010-4655(95)00042-E.

Cheng, Yifan. 2018. “Membrane Protein Structural Biology in the Era of Single Particle Cryo-EM.” *Current Opinion in Structural Biology*. Elsevier Ltd. https://doi.org/10.1016/j.sbi.2018.08.008.

Chevallet, Mireille, Sylvie Luche, and Thierry Rabilloud. 2006. “Silver Staining of Proteins in Polyacrylamide Gels.” *Nature Protocols* 1 (4): 1852–58. https://doi.org/10.1038/nprot.2006.288.

com/, M Frisch - http://www. gaussian., and undefined 2009. n.d. “Gaussian09.” *Ci.Nii.Ac.Jp*. Accessed January 30, 2021. https://ci.nii.ac.jp/naid/10030878110/.

Conway, Patrick, Michael D. Tyka, Frank DiMaio, David E. Konerding, and David Baker. 2014. “Relaxation of Backbone Bond Geometry Improves Protein Energy Landscape Modeling.” *Protein Science* 23 (1): 47–55. https://doi.org/10.1002/pro.2389.

Dasa, Rhiju, Ingemar André, Yang Shen, Yibing Wu, Alexander Lemak, Sonal Bansal, Cheryl H. Arrowsmith, Thomas Szyperski, and David Baker. 2009. “Simultaneous Prediction of Protein Folding and Docking at High Resolution.” *Proceedings of the National Academy of Sciences of the United States of America* 106 (45): 18978–83. https://doi.org/10.1073/pnas.0904407106.

Donato, Rosario. 1999. “Functional Roles of S100 Proteins, Calcium-Binding Proteins of the EF-Hand Type.” *Biochimica et Biophysica Acta - Molecular Cell Research*. Elsevier. https://doi.org/10.1016/S0167-4889(99)00058-0.

Donnelly, Daniel P., Catherine M. Rawlins, Caroline J. DeHart, Luca Fornelli, Luis F. Schachner, Ziqing Lin, Jennifer L. Lippens, et al. 2019. “Best Practices and Benchmarks for Intact Protein Analysis for Top-down Mass Spectrometry.” *Nature Methods* 16 (7): 587–94. https://doi.org/10.1038/s41592-019-0457-0.

Fang, Lih Fen Lue, Shiqiang Yan, Hongwei Xu, John S. Luddy, Doris Chen, Douglas G. Walker, et al. 2010. “RAGE-Dependent Signaling in Microglia Contributes to Neuroinflammation, Aβ Accumulation, and Impaired Learning/Memory in a Mouse Model of Alzheimer’s Disease.” *FASEB Journal* 24 (4): 1043–55. https://doi.org/10.1096/fj.09-139634.

Gault, Joseph, Joseph A.C. Donlan, Idlir Liko, Jonathan T.S. Hopper, Kallol Gupta, Nicholas G. Housden, Weston B. Struwe, et al. 2016. “High-Resolution Mass Spectrometry of Small Molecules Bound to Membrane Proteins.” *Nature Methods* 13 (4): 333–36. https://doi.org/10.1038/nmeth.3771.

Götze, Michael, Jens Pettelkau, Romy Fritzsche, Christian H. Ihling, Mathias Schäfer, and Andrea Sinz. 2014. “Automated Assignment of MS/MS Cleavable Cross-Links in Protein 3d-Structure Analysis.” *Journal of the American Society for Mass Spectrometry* 26 (1): 83–97. https://doi.org/10.1007/s13361-014-1001-1.

Guex, Nicolas, and Manuel C. Peitsch. 1997. “SWISS-MODEL and the Swiss-PdbViewer: An Environment for Comparative Protein Modeling.” *Electrophoresis* 18 (15): 2714–23. https://doi.org/10.1002/elps.1150181505.

Huang, Jing, and Alexander D. Mackerell. 2013. “CHARMM36 All-Atom Additive Protein Force Field: Validation Based on Comparison to NMR Data.” *Journal of Computational Chemistry* 34 (25): 2135–45. https://doi.org/10.1002/jcc.23354.

Huang, Po Ssu, Yih En Andrew Ban, Florian Richter, Ingemar Andre, Robert Vernon, William R. Schief, and David Baker. 2011. “Rosettaremodel: A Generalized Framework for Flexible Backbone Protein Design.” *PLoS ONE* 6 (8). https://doi.org/10.1371/journal.pone.0024109.

Hudson, Barry I., Anastasia Z. Kalea, Maria Del Mar Arriero, Evis Harja, Eric Boulanger, Vivette D’Agati, and Ann Marie Schmidt. 2008. “Interaction of the RAGE Cytoplasmic Domain with Diaphanous-1 Is Required for Ligand-Stimulated Cellular Migration through Activation of Rac1 and Cdc42.” *Journal of Biological Chemistry* 283 (49): 34457–68. https://doi.org/10.1074/jbc.M801465200.

Hurwitz, Shmuel. 1996. “Homeostatic Control of Plasma Calcium Concentration.” *Critical Reviews in Biochemistry and Molecular Biology*. Informa Healthcare. https://doi.org/10.3109/10409239609110575.

Huttunen, Henri J., Juha Kuja-Panula, Guglielmo Sorci, Anna Lisa Agneletti, Rosario Donato, and Heikki Rauvala. 2000. “Coregulation of Neurite Outgrowth and Cell Survival by Amphoterin and S100 Proteins through Receptor for Advanced Glycation End Products (RAGE) Activation.” *Journal of Biological Chemistry* 275 (51): 40096–105. https://doi.org/10.1074/jbc.M006993200.

Huttunen, Henri J, Carole Fages, Juha Kuja-Panula, Anne J Ridley, and Heikki Rauvala. 2002. “Receptor for Advanced Glycation End Products-Binding COOH-Terminal Motif of Amphoterin Inhibits Invasive Migration and Metastasis.” *Cancer Research* 62 (16): 4805–11.

Ishihara, Katsuya, Kae Tsutsumi, Shiho Kawane, Motowo Nakajima, and Tatsuhiko Kasaoka. 2003. “The Receptor for Advanced Glycation End-Products (RAGE) Directly Binds to ERK by a D-Domain-like Docking Site.” *FEBS Letters* 550 (1–3): 107–13. https://doi.org/10.1016/S0014-5793(03)00846-9.

Jensen, Jaime L., Venkata S.K. Indurthi, David B. Neau, Stefan W. Vetter, and Christopher L. Colbert. 2015. “Structural Insights into the Binding of the Human Receptor for Advanced Glycation End Products (RAGE) by S100B, as Revealed by an S100B-RAGE-Derived Peptide Complex.” *Acta Crystallographica Section D: Biological Crystallography* 71 (Pt 5): 1176–83. https://doi.org/10.1107/S1399004715004216.

Juranek, Judyta K., Gurdip K. Daffu, Matthew S. Geddis, Huilin Li, Rosa Rosario, Benjamin J. Kaplan, Lauren Kelly, and Ann Marie Schmidt. 2016. “Soluble RAGE Treatment Delays Progression of Amyotrophic Lateral Sclerosis in SOD1 Mice.” *Frontiers in Cellular Neuroscience* 10 (MAY). https://doi.org/10.3389/fncel.2016.00117.

Kleiger, Gary, Robert Grothe, Parag Mallick, and David Eisenberg. 2002. “GXXXG and AXXXA: Common Alpha-Helical Interaction Motifs in Proteins, Particularly in Extremophiles.” *Biochemistry* 41 (19): 5990–97. http://www.ncbi.nlm.nih.gov/pubmed/11993993.

Koch, Michael, Seth Chitayat, Brian M Dattilo, Andre Schiefner, Joachim Diez, Walter J Chazin, and Gunter Fritz. 2010. “Structural Basis for Ligand Recognition and Activation of RAGE.” *Structure (London, England : 1993)* 18 (10): 1342–52. https://doi.org/10.1016/j.str.2010.05.017.

Laure Yatime, Authors, Cristine Betzer, Rasmus Kjeldsen Jensen, Sofia Mortensen, Poul Henning Jensen, Gregers Rom Andersen, and Laure Yatime. 2016. “The Structure of the RAGE:S100A6 Complex Reveals a Unique Mode of Homodimerization for S100 Proteins In Brief Accession Numbers 4P2Y 4YBH The Structure of the RAGE:S100A6 Complex Reveals a Unique Mode of Homodimerization for S100 Proteins.” https://doi.org/10.1016/j.str.2016.09.011.

Leclerc, Estelle, Günter Fritz, Stefan W. Vetter, and Claus W. Heizmann. 2009. “Binding of S100 Proteins to RAGE: An Update.” *Biochimica et Biophysica Acta - Molecular Cell Research*. https://doi.org/10.1016/j.bbamcr.2008.11.016.

Leclerc, Estelle, Emmanuel Sturchler, and Stefan W. Vetter. 2010. “The S100B/RAGE Axis in Alzheimer’s Disease.” *Cardiovascular Psychiatry and Neurology*. https://doi.org/10.1155/2010/539581.

Lee, Jumin, Dhilon S. Patel, Jonas Ståhle, Sang Jun Park, Nathan R. Kern, Seonghoon Kim, Joonseong Lee, et al. 2019. “CHARMM-GUI Membrane Builder for Complex Biological Membrane Simulations with Glycolipids and Lipoglycans.” *Journal of Chemical Theory and Computation* 15 (1): 775–86. https://doi.org/10.1021/acs.jctc.8b01066.

Leney, Aneika C, and Albert J R Heck. 2017. “Native Mass Spectrometry: What Is in the Name?” *Journal of the American Society for Mass Spectrometry* 28 (1): 5–13. https://doi.org/10.1007/s13361-016-1545-3.

Lindorff-Larsen, Kresten, Stefano Piana, Kim Palmo, Paul Maragakis, John L. Klepeis, Ron O. Dror, and David E. Shaw. 2010. “Improved Side-Chain Torsion Potentials for the Amber Ff99SB Protein Force Field.” *Proteins: Structure, Function and Bioinformatics* 78 (8): 1950–58. https://doi.org/10.1002/prot.22711.

MacLean, Michael, Julia Derk, Henry H. Ruiz, Judyta K. Juranek, Ravichandran Ramasamy, and Ann Marie Schmidt. 2019. “The Receptor for Advanced Glycation End Products (RAGE) and DIAPH1: Implications for Vascular and Neuroinflammatory Dysfunction in Disorders of the Central Nervous System.” *Neurochemistry International*. Elsevier Ltd. https://doi.org/10.1016/j.neuint.2019.03.012.

Manigrasso, Michaele B, Jinhong Pan, Vivek Rai, Jinghua Zhang, Sergey Reverdatto, Nosirudeen Quadri, Robert J DeVita, Ravichandran Ramasamy, Alexander Shekhtman, and Ann Marie Schmidt. 2016. “Small Molecule Inhibition of Ligand-Stimulated RAGE-DIAPH1 Signal Transduction.” *Scientific Reports* 6 (March): 22450. https://doi.org/10.1038/srep22450.

Marty, Michael T., Andrew J. Baldwin, Erik G. Marklund, Georg K.A. Hochberg, Justin L.P. Benesch, and Carol V. Robinson. 2015. “Bayesian Deconvolution of Mass and Ion Mobility Spectra: From Binary Interactions to Polydisperse Ensembles.” *Analytical Chemistry* 87 (8): 4370–76. https://doi.org/10.1021/acs.analchem.5b00140.

Mendes, Marta L, Lutz Fischer, Zhuo A Chen, Marta Barbon, Francis J O’Reilly, Sven H Giese, Michael Bohlke-Schneider, et al. 2019. “An Integrated Workflow for Crosslinking Mass Spectrometry.” *Molecular Systems Biology* 15 (9). https://doi.org/10.15252/msb.20198994.

Merkley, Eric D., Steven Rysavy, Abdullah Kahraman, Ryan P. Hafen, Valerie Daggett, and Joshua N. Adkins. 2014. “Distance Restraints from Crosslinking Mass Spectrometry: Mining a Molecular Dynamics Simulation Database to Evaluate Lysine-Lysine Distances.” *Protein Science* 23 (6): 747–59. https://doi.org/10.1002/pro.2458.

Michetti, Fabrizio, Nadia D’Ambrosi, Amelia Toesca, Maria Ausiliatrice Puglisi, Alessia Serrano, Elisa Marchese, Valentina Corvino, and Maria Concetta Geloso. 2019. “The S100B Story: From Biomarker to Active Factor in Neural Injury.” *Journal of Neurochemistry*. Blackwell Publishing Ltd. https://doi.org/10.1111/jnc.14574.

Moldogazieva, Nurbubu T., Innokenty M. Mokhosoev, Tatiana I. Mel’nikova, Yuri B. Porozov, and Alexander A. Terentiev. 2019. “Oxidative Stress and Advanced Lipoxidation and Glycation End Products (ALEs and AGEs) in Aging and Age-Related Diseases.” *Oxidative Medicine and Cellular Longevity*. NLM (Medline). https://doi.org/10.1155/2019/3085756.

Moysa, Alexander, Dietmar Hammerschmid, Roman H. Szczepanowski, Frank Sobott, and Michal Dadlez. 2019. “Enhanced Oligomerization of Full-Length RAGE by Synergy of the Interaction of Its Domains.” *Scientific Reports* 9 (1): 20332. https://doi.org/10.1038/s41598-019-56993-9.

Neeper, M., A. M. Schmidt, J. Brett, Shi Du Yan, F. Wang, Y. C.E. Pan, K. Elliston, D. Stern, and A. Shaw. 1992. “Cloning and Expression of a Cell Surface Receptor for Advanced Glycosylation End Products of Proteins.” *Journal of Biological Chemistry* 267 (21): 14998–4.

Ni, Mao Wei, Lu Wang, Wei Chen, Han Zhou Mou, Jie Zhou, and Zhi Guo Zheng. 2017. “Modified Filter-Aided Sample Preparation (FASP) Method Increases Peptide and Protein Identifications for Shotgun Proteomics.” *Rapid Communications in Mass Spectrometry* 31 (2): 171–78. https://doi.org/10.1002/rcm.7779.

Nivón, Lucas Gregorio, Rocco Moretti, and David Baker. 2013. “A Pareto-Optimal Refinement Method for Protein Design Scaffolds.” *PLoS ONE* 8 (4). https://doi.org/10.1371/journal.pone.0059004.

Nter Fritz, Gü. 2011. “RAGE: A Single Receptor Fits Multiple Ligands.” *Trends in Biochemical Sciences* 36 (12): 625–32. https://doi.org/10.1016/j.tibs.2011.08.008.

Olubiyi, Olujide O., and Birgit Strodel. 2012. “Structures of the Amyloid β-Peptides Aβ1-40 and Aβ1-42 as Influenced by PH and a d-Peptide.” *Journal of Physical Chemistry B* 116 (10): 3280–91. https://doi.org/10.1021/jp2076337.

Ostendorp, Thorsten, Estelle Leclerc, Arnaud Galichet, Michael Koch, Nina Demling, Bernd Weigle, Claus W. Heizmann, Peter M.H. Kroneck, and Günter Fritz. 2007. “Structural and Functional Insights into RAGE Activation by Multimeric S100B.” *EMBO Journal* 26 (16): 3868–78. https://doi.org/10.1038/sj.emboj.7601805.

Park, Su Yeon, Young A. Kim, Yoon Ho Hong, Min Kyong Moon, Bo Kyeong Koo, and Tae Wan Kim. 2014. “Up-Regulation of the Receptor for Advanced Glycation End Products in the Skin Biopsy Specimens of Patients with Severe Diabetic Neuropathy.” *Journal of Clinical Neurology (Korea)* 10 (4): 334–41. https://doi.org/10.3988/jcn.2014.10.4.334.

Pietzsch, Jens. 2011. “S100 Proteins in Health and Disease.” *Amino Acids*. Amino Acids. https://doi.org/10.1007/s00726-010-0816-8.

Puchała, Weronika, Michał Burdukiewicz, Michał Kistowski, Katarzyna A Dąbrowska, Aleksandra E Badaczewska-Dawid, Dominik Cysewski, and Michał Dadlez. 2020. “HaDeX: An R Package and Web-Server for Analysis of Data from Hydrogen–Deuterium Exchange Mass Spectrometry Experiments.” Edited by Yann Ponty. *Bioinformatics* 36 (16): 4516–18. https://doi.org/10.1093/bioinformatics/btaa587.

Rai, Vivek, Andres Y. Maldonado, David S. Burz, Sergey Reverdatto, Ann Marie Schmidt, and Alexander Shekhtman. 2012. “Signal Transduction in Receptor for Advanced Glycation End Products (RAGE): Solution Structure of C-Terminal Rage (CtRAGE) and Its Binding to MDia1.” *Journal of Biological Chemistry* 287 (7): 5133–44. https://doi.org/10.1074/jbc.M111.277731.

Riehl, Astrid, Tobias Bauer, Benedikt Brors, Hauke Busch, Regina Mark, Julia Németh, Christoffer Gebhardt, et al. 2010. “Identification of the Rage-Dependent Gene Regulatory Network in a Mouse Model of Skin Inflammation.” *BMC Genomics* 11 (1). https://doi.org/10.1186/1471-2164-11-537.

Sakaguchi, Masakiyo, Hitoshi Murata, Ken ichi Yamamoto, Tomoyuki Ono, Yoshihiko Sakaguchi,

Akira Motoyama, Toshihiko Hibino, Ken Kataoka, and Nam ho Huh. 2011. “TIRAP, an Adaptor Protein for TLR2/4, Transduces a Signal from RAGE Phosphorylated upon Ligand Binding.” *PLoS ONE* 6 (8). https://doi.org/10.1371/journal.pone.0023132.

Schrodinger LLC. 2015. “The PyMOL Molecular Graphics System, Version 1.8.”

Sedaghat, F., and A. Notopoulos. 2008. “S100 Protein Family and Its Application in Clinical Practice.” *Hippokratia*. Hippokratio General Hospital of Thessaloniki.

Smith, Colin A., and Tanja Kortemme. 2008. “Backrub-Like Backbone Simulation Recapitulates Natural Protein Conformational Variability and Improves Mutant Side-Chain Prediction.” *Journal of Molecular Biology* 380 (4): 742–56. https://doi.org/10.1016/j.jmb.2008.05.023.

Smith, Steven P., and Gary S. Shaw. 1998. “A Change-in-Hand Mechanism for S100 Signalling.” *Biochemistry and Cell Biology* 76 (2–3): 324–33. https://doi.org/10.1139/bcb-76-2-3-324.

Streicher, Werner W., Maria M. Lopez, and George I. Makhatadze. 2010. “Modulation of Quaternary Structure of S100 Proteins by Calcium Ions.” *Biophysical Chemistry* 151 (3): 181–86. https://doi.org/10.1016/j.bpc.2010.06.003.

Taub, Chloe J., Marc E. Lippman, Barry I. Hudson, Bonnie B. Blomberg, Alain Diaz, Hannah M. Fisher, Erica R. Nahin, et al. 2019. “The Effects of a Randomized Trial of Brief Forms of Stress Management on RAGE-Associated S100A8/A9 in Patients with Breast Cancer Undergoing Primary Treatment.” *Cancer* 125 (10): 1717–25. https://doi.org/10.1002/cncr.31965.

Teese, Mark G., and Dieter Langosch. 2015. “Role of GxxxG Motifs in Transmembrane Domain Interactions.” *Biochemistry* 54 (33): 5125–35. https://doi.org/10.1021/acs.biochem.5b00495.

Thulin, Eva, Tõnu Kesvatera, and Sara Linse. 2011. “Molecular Determinants of S100B Oligomer Formation.” *PLoS ONE* 6 (3). https://doi.org/10.1371/journal.pone.0014768.

Vangone, Anna, Raffaele Spinelli, Vittorio Scarano, Luigi Cavallo, and Romina Oliva. 2011. “COCOMAPS: A Web Application to Analyze and Visualize Contacts at the Interface of Biomolecular Complexes.” *Bioinformatics*. Oxford Academic. https://doi.org/10.1093/bioinformatics/btr484.

Villarreal, Alejandro, Rocío Seoane, Agustina González Torres, Gerardo Rosciszewski, Maria Florencia Angelo, Alicia Rossi, Philip A. Barkert, and Alberto Javier Ramos. 2014. “S100B Protein Activates a RAGE-Dependent Autocrine Loop in Astrocytes: Implications for Its Role in the Propagation of Reactive Gliosis.” *Journal of Neurochemistry* 131 (2): 190–205. https://doi.org/10.1111/jnc.12790.

Wei, Wen, Leonie Lampe, Sungha Park, Bhavana S Vangara, Geoffrey S Waldo, Stephanie Cabantous, Sarah S Subaran, Dongmei Yang, Edward G Lakatta, and Li Lin. 2012. “Disulfide Bonds within the C2 Domain of RAGE Play Key Roles in Its Dimerization and Biogenesis.” *PloS One* 7 (12): e50736. https://doi.org/10.1371/journal.pone.0050736.

Winkler, Robert. 2010. “ESIprot: A Universal Tool for Charge State Determination and Molecular Weight Calculation of Proteins from Electrospray Ionization Mass Spectrometry Data.” *Rapid Communications in Mass Spectrometry* 24 (3): 285–94. https://doi.org/10.1002/rcm.4384.

Wu, Hao. 2013. “Higher-Order Assemblies in a New Paradigm of Signal Transduction.” *Cell*. Cell Press. https://doi.org/10.1016/j.cell.2013.03.013.

Xie, Jingjing, David S Burz, Wei He, Igor B Bronstein, Igor Lednev, and Alexander Shekhtman. 2007. “Hexameric Calgranulin C (S100A12) Binds to the Receptor for Advanced Glycated End Products (RAGE) Using Symmetric Hydrophobic Target-Binding Patches.” *The Journal of Biological Chemistry* 282 (6): 4218–31. https://doi.org/10.1074/jbc.M608888200.

Xu, Ding, Jeffrey H Young, Juno M Krahn, Danyin Song, Kevin D Corbett, Walter J Chazin, Lars C Pedersen, and Jeffrey D Esko. 2013. “Stable RAGE-Heparan Sulfate Complexes Are Essential for Signal Transduction.” *ACS Chemical Biology* 8 (7): 1611–20. https://doi.org/10.1021/cb4001553.

Xue, Jing, Michaele Manigrasso, Matteo Scalabrin, Vivek Rai, Sergey Reverdatto, David S. Burz, Daniele Fabris, Ann Marie Schmidt, and Alexander Shekhtman. 2016. “Change in the Molecular Dimension of a RAGE-Ligand Complex Triggers RAGE Signaling.” *Structure* 24 (9): 1509–22. https://doi.org/10.1016/J.STR.2016.06.021.

Xue, Jing, Vivek Rai, David Singer, Stefan Chabierski, Jingjing Xie, Sergey Reverdatto, David S Burz, Ann Marie Schmidt, Ralf Hoffmann, and Alexander Shekhtman. 2011. “Advanced Glycation End Product Recognition by the Receptor for AGEs.” *Structure (London, England : 1993)* 19 (5): 722–32. https://doi.org/10.1016/j.str.2011.02.013.

Yamamoto, Ken Ichi, Hitoshi Murata, Endy Widya Putranto, Ken Kataoka, Akira Motoyama, Toshihiko Hibino, Yusuke Inoue, Masakiyo Sakaguchi, and Nam Ho Huh. 2013. “DOCK7 Is a Critical Regulator of the RAGE-Cdc42 Signaling Axis That Induces Formation of Dendritic Pseudopodia in Human Cancer Cells.” *Oncology Reports* 29 (3): 1073–79.

https://doi.org/10.3892/or.2012.2191.
Yan, S D, D Stern, M D Kane, Y M Kuo, H C Lampert, and A E Roher. 1998. “RAGE-Abeta Interactions in the Pathophysiology of Alzheimer’s Disease.” *Restorative Neurology and Neuroscience* 12 (2–3): 167–73. http://www.ncbi.nlm.nih.gov/pubmed/12671312.
Yan, Shi Fang, Ravichandran Ramasamy, and Ann Marie Schmidt. 2009. “The Receptor for Advanced Glycation Endproducts (RAGE) and Cardiovascular Disease.” *Expert Reviews in Molecular Medicine*. https://doi.org/10.1017/S146239940900101X.
Yatime, Laure, and Gregers R Andersen. 2013. “Structural Insights into the Oligomerization Mode of the Human Receptor for Advanced Glycation End-Products.” *The FEBS Journal* 280 (24): 6556–68. https://doi.org/10.1111/febs.12556.
Yatime, Laure, and Gregers Rom Andersen. 2014. “The Specificity of DNA Recognition by the RAGE Receptor.” *The Journal of Experimental Medicine*. United States. https://doi.org/10.1084/jem.20132526.
Yatime, Laure, Cristine Betzer, Rasmus Kjeldsen Jensen, Sofia Mortensen, Poul Henning Jensen, and Gregers Rom Andersen. 2016. “The Structure of the RAGE:S100A6 Complex Reveals a Unique Mode of Homodimerization for S100 Proteins.” *Structure (London, England : 1993)* 24 (12): 2043–52. https://doi.org/10.1016/j.str.2016.09.011.
Yin, Chonggao, Hongli Li, Baogang Zhang, Yuqing Liu, Guohua Lu, Shijun Lu, Lei Sun, Yueliang Qi, Xiaolong Li, and Weiyi Chen. 2013. “RAGE-Binding S100A8/A9 Promotes the Migration and Invasion of Human Breast Cancer Cells through Actin Polymerization and Epithelial-Mesenchymal Transition.” *Breast Cancer Research and Treatment* 142 (2): 297–309. https://doi.org/10.1007/s10549-013-2737-1.
Yu, Clinton, and Lan Huang. 2018. “Cross-Linking Mass Spectrometry: An Emerging Technology for Interactomics and Structural Biology.” *Analytical Chemistry*. American Chemical Society. https://doi.org/10.1021/acs.analchem.7b04431.
Zhang, Hongju, Yongfu Wang, Shijun Yan, Fang Du, Long Wu, Shiqiang Yan, and Shirley S. Yan. 2014. “Genetic Deficiency of Neuronal RAGE Protects against AGE-Induced Synaptic Injury.” *Cell Death and Disease* 5 (6). https://doi.org/10.1038/cddis.2014.248.
Zhukova, Liliya, Igor Zhukov, Wojciech Bal, and Aleksandra Wyslouch-Cieszynska. 2004. “Redox Modifications of the C-Terminal Cysteine Residue Cause Structural Changes in S100A1 and S100B Proteins.” In *Biochimica et Biophysica Acta - Molecular Cell Research*, 1742:191–201. Elsevier. https://doi.org/10.1016/j.bbamcr.2004.10.002.
Zong, Hongliang, Angelina Madden, Micheal Ward, Mark H Mooney, Christopher T Elliott, and Alan W Stitt. 2010. “Homodimerization Is Essential for the Receptor for Advanced Glycation End Products (RAGE)-Mediated Signal Transduction.” *The Journal of Biological Chemistry* 285 (30): 23137–46. https://doi.org/10.1074/jbc.M110.133827.

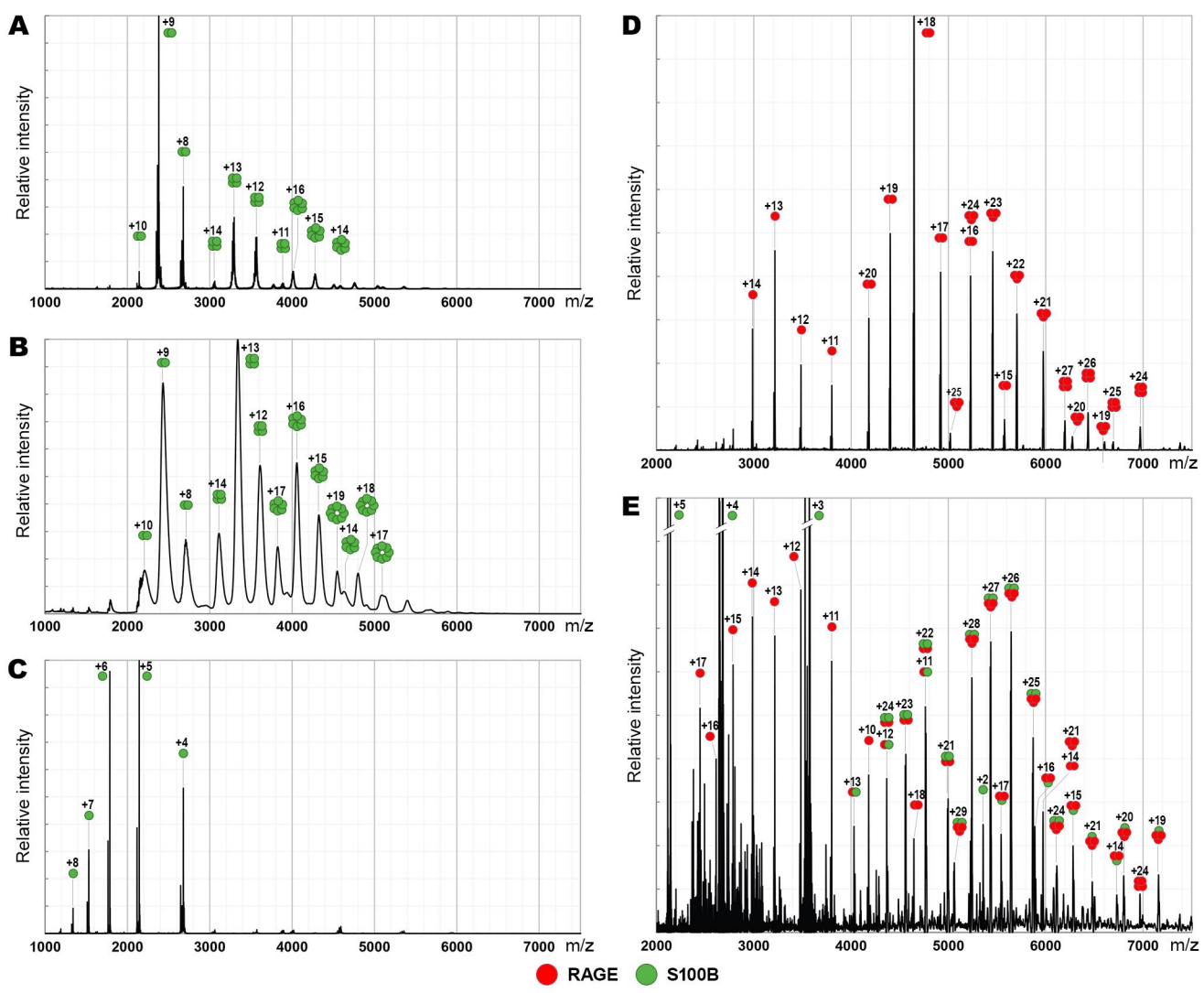
A
B
C
D
E
Relative intensity
m/z
1000
2000
3000
4000
5000
6000
7000
RAGE
S100B

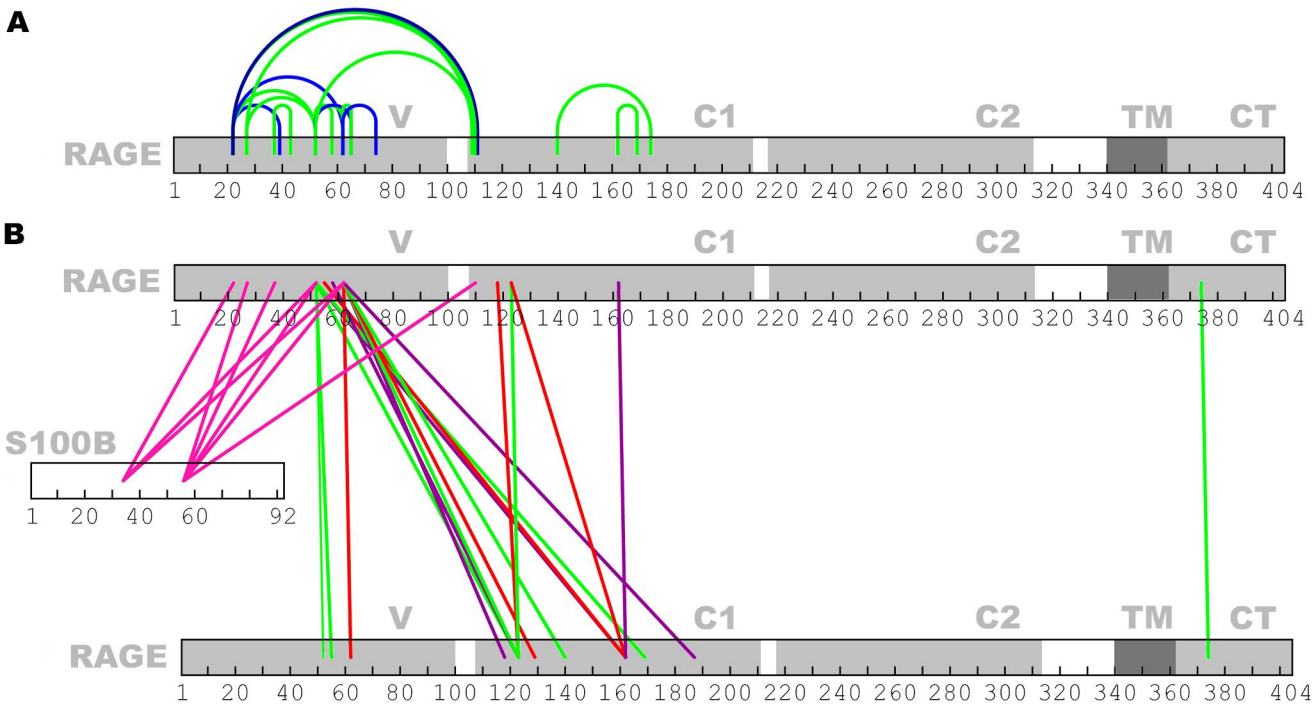
A
V
C1
C2
TM
CT
RAGE
1 20 40 60 80 100 120 140 160 180 200 220 240 260 280 300 320 340 360 380 404
B
V
C1
C2
TM
CT
RAGE
1 20 40 60 80 100 120 140 160 180 200 220 240 260 280 300 320 340 360 380 404
S100B
1 20 40 60 92
V
C1
C2
TM
CT
RAGE
1 20 40 60 80 100 120 140 160 180 200 220 240 260 280 300 320 340 360 380 404

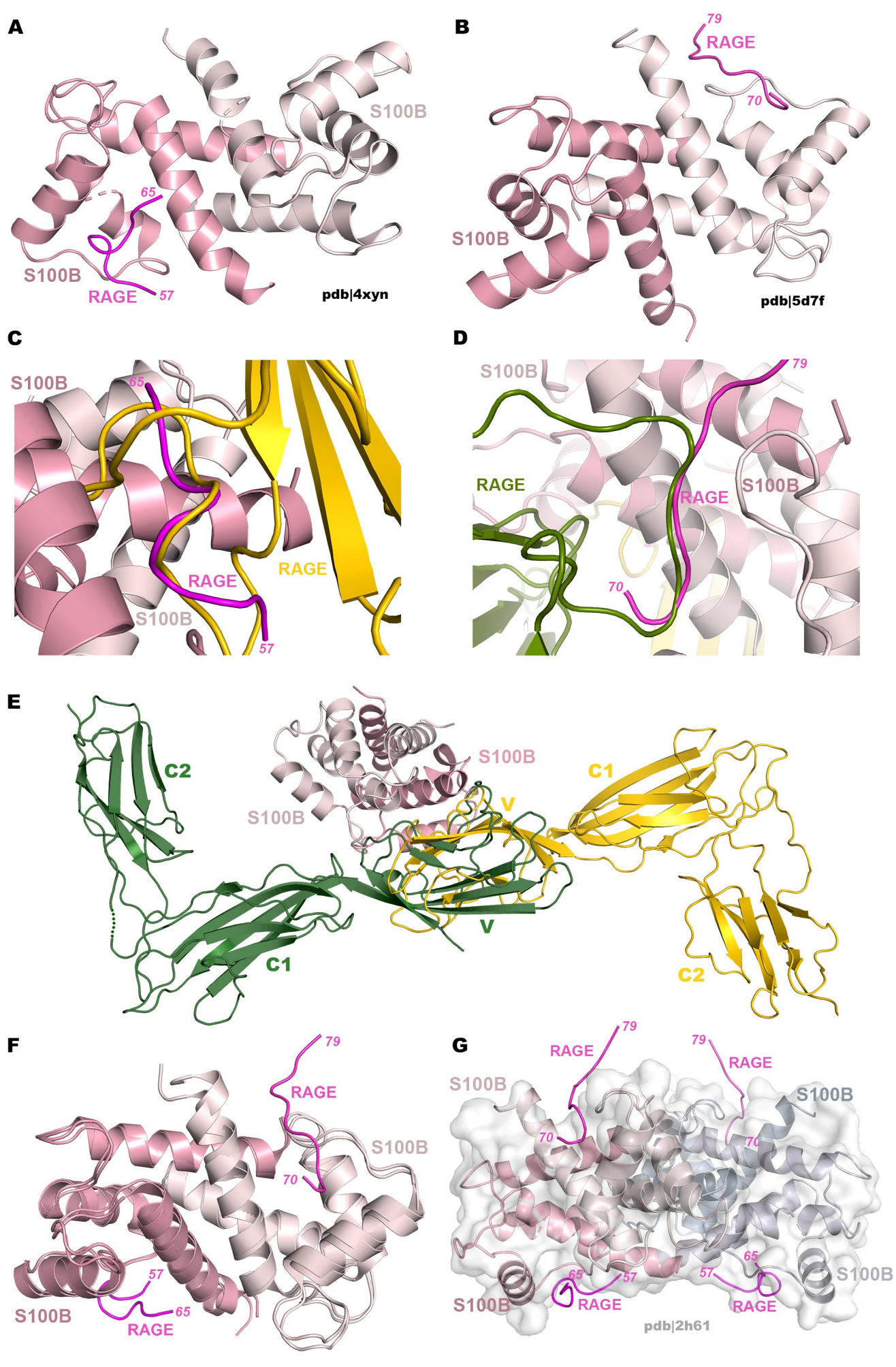
A
S100B
65
S100B
RAGE
57
pdb|4xyn
B
79
RAGE
70
S100B
pdb|5d7f
C
S100B
65
RAGE
RAGE
S100B
57
D
S100B
79
RAGE
RAGE
S100B
70
E
C2
S100B
S100B
V
C1
V
C1
C2
F
79
RAGE
S100B
70
57
S100B
65
RAGE
G
79
RAGE
79
RAGE
S100B
S100B
70
70
65
57
57
65
S100B
S100B
RAGE
RAGE
pdb|2h61

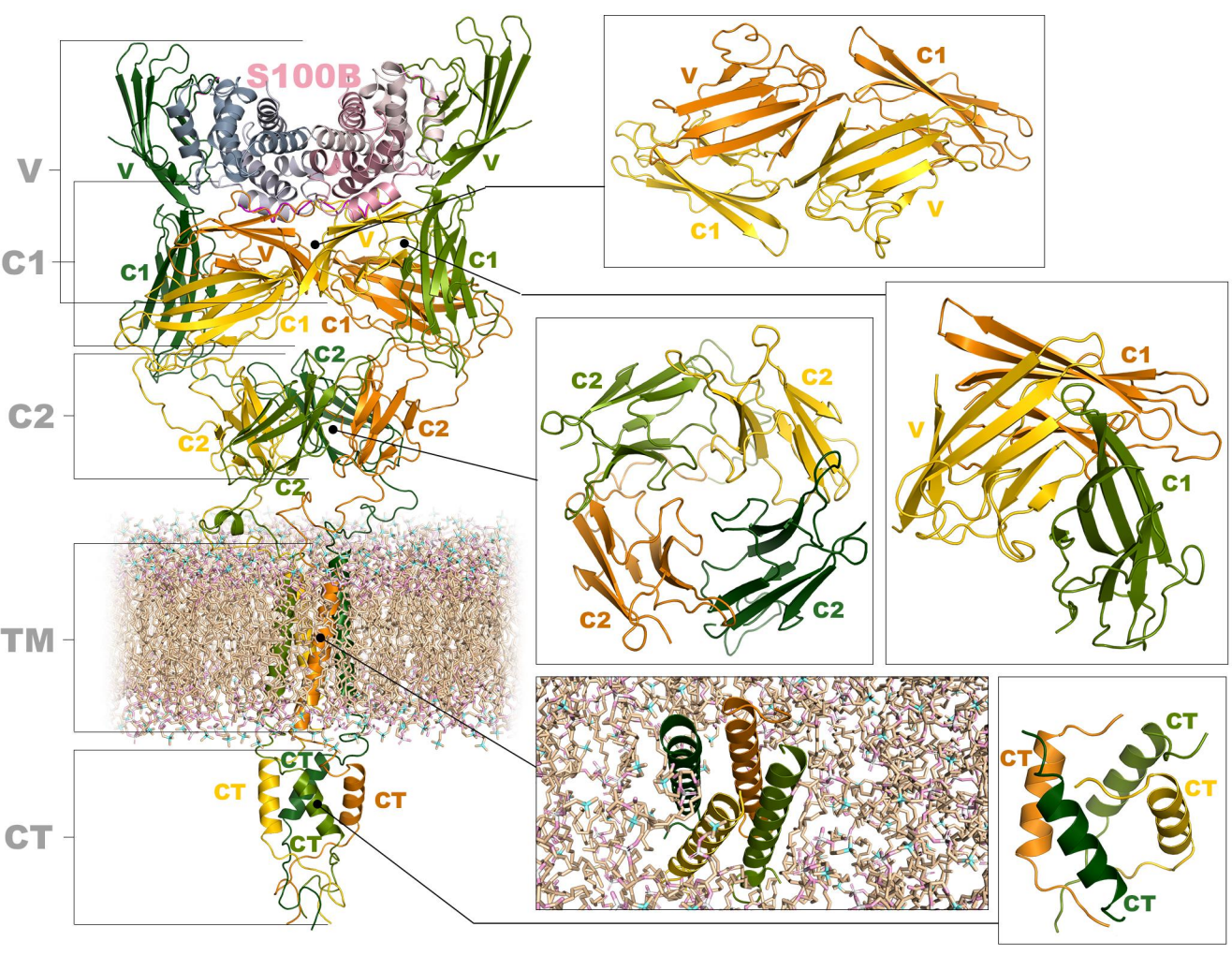
S100B
V
C1
C2
TM
CT
V
V
V
V
C1
C1
C1
C1
C2
C2
C2
C2
CT
CT
CT
CT
V
C1
C1
V
C2
C2
C2
C2
V
C1
C1
CT
CT
CT
CT

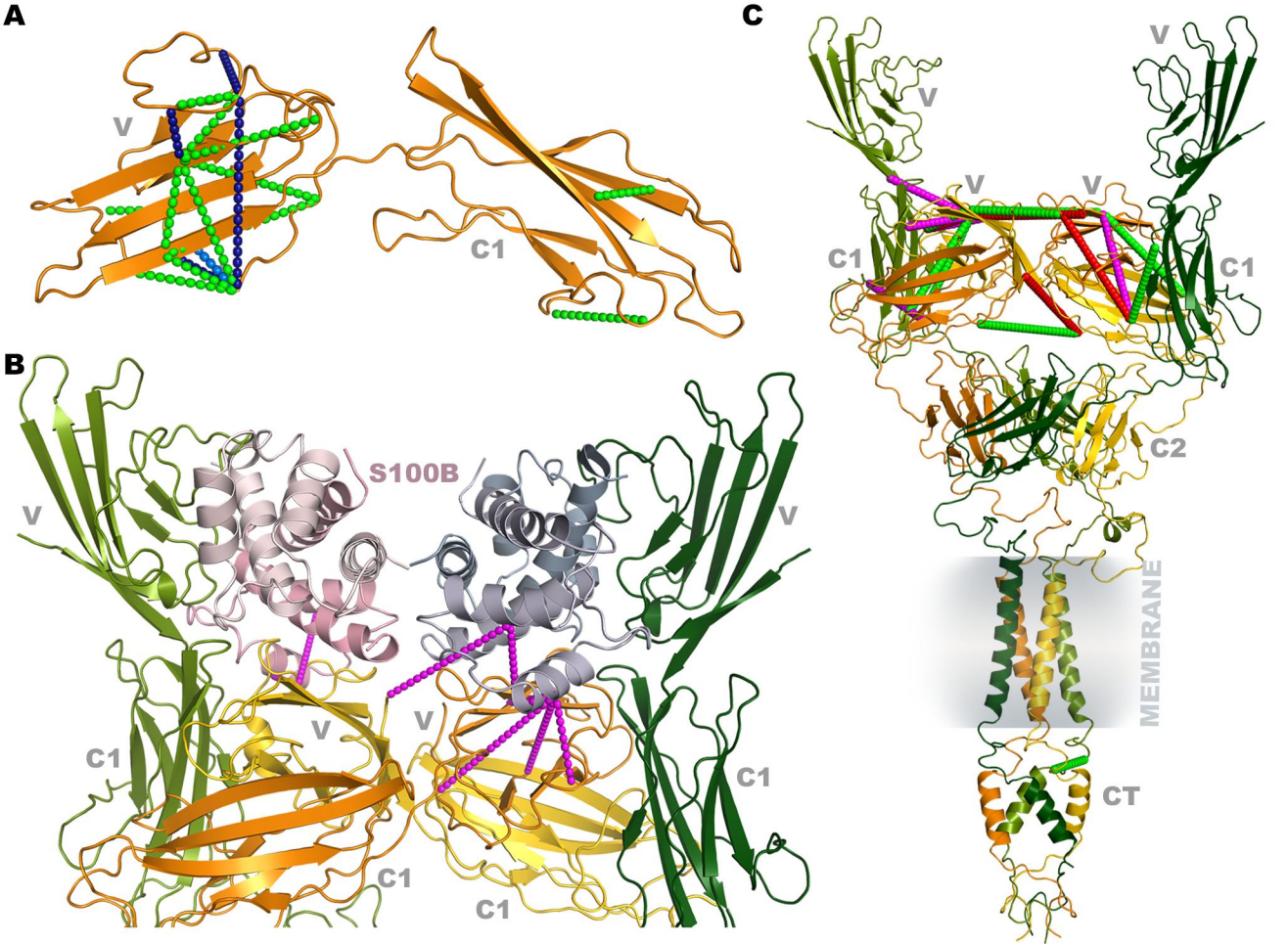
A
V
C1
B
S100B
V
V
V
V
C1
C1
C1
C1
C
V
V
V
V
C1
C1
C2
MEMBRANE
CT

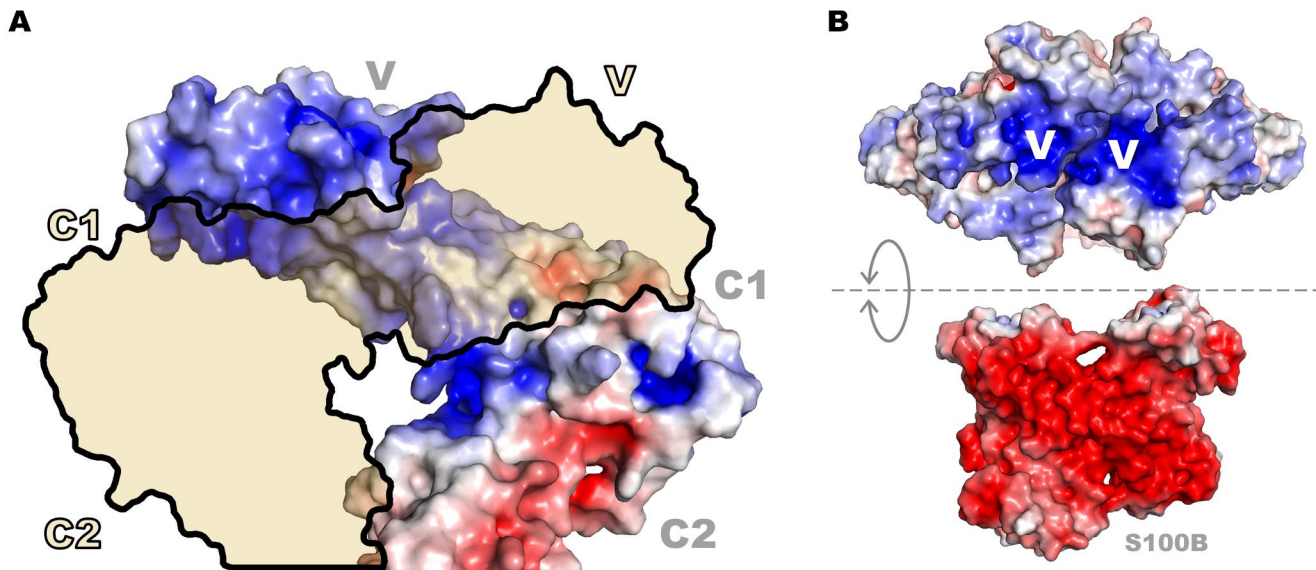
A
V
V
C1
C1
C2
C2
B
V
V
S100B

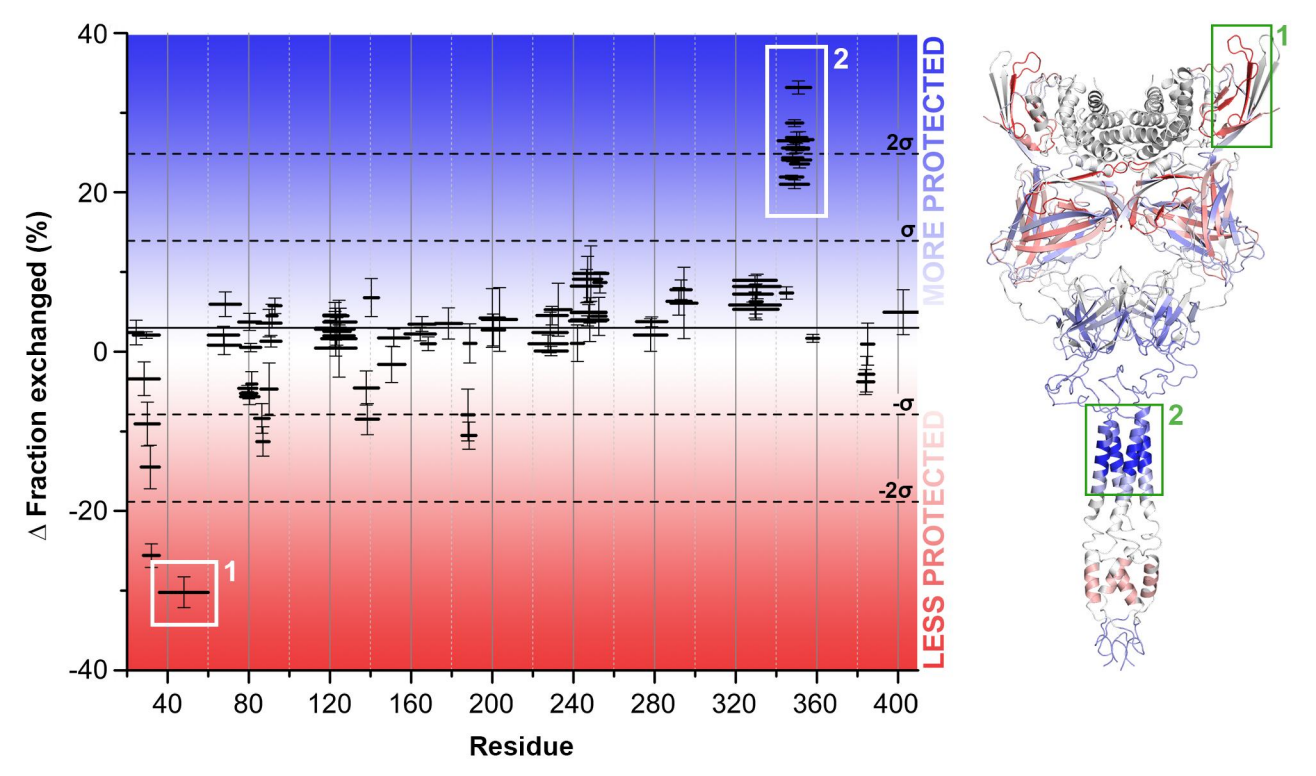
40
20
0
-20
-40
Δ Fraction exchanged (%)
40
80
120
160
200
240
280
320
360
400
Residue
2σ
σ
-σ
-2σ
MORE PROTECTED
LESS PROTECTED
1
2
1
2

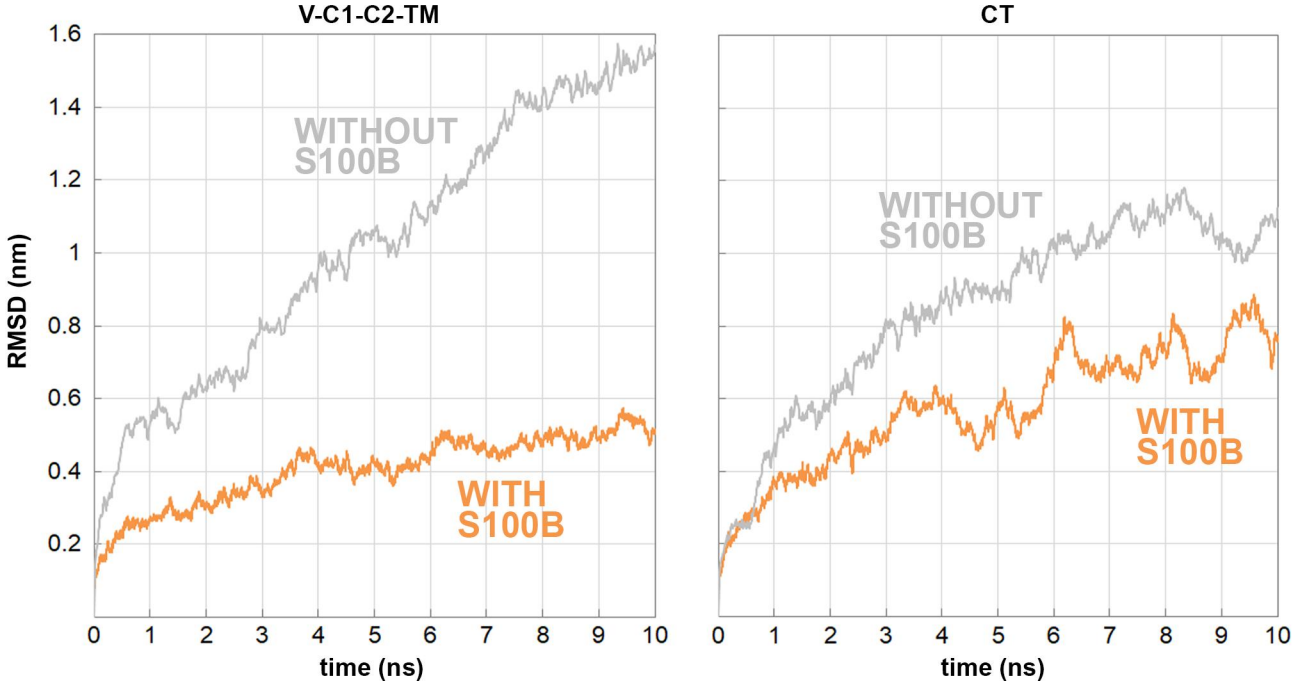
V-C1-C2-TM
CT
RMSD (nm)
1.6
1.4
1.2
1
0.8
0.6
0.4
0.2
WITHOUT S100B
WITH S100B
WITHOUT S100B
WITH S100B
0 1 2 3 4 5 6 7 8 9 10
time (ns)
0 1 2 3 4 5 6 7 8 9 10
time (ns)

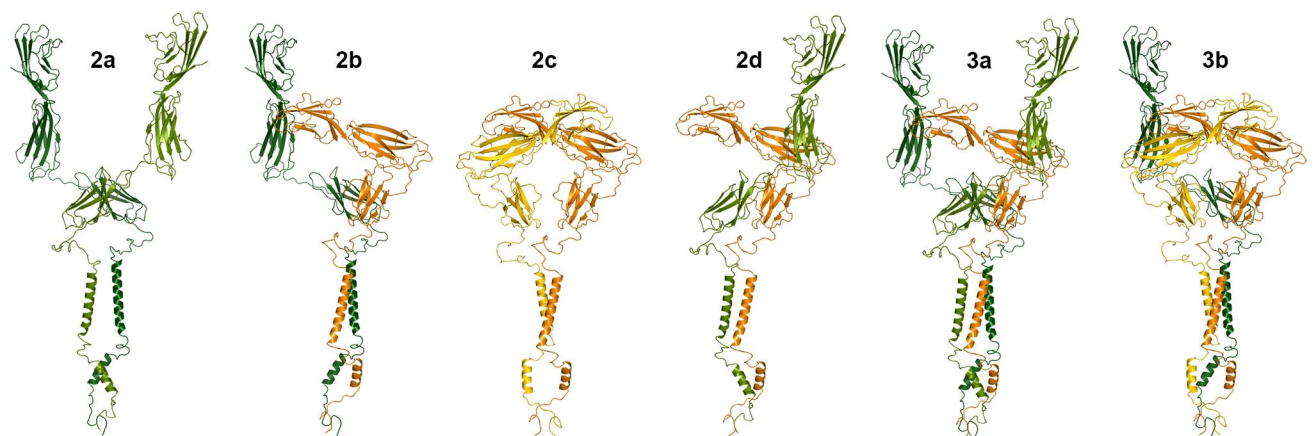
2a
2b
2c
2d
3a
3b

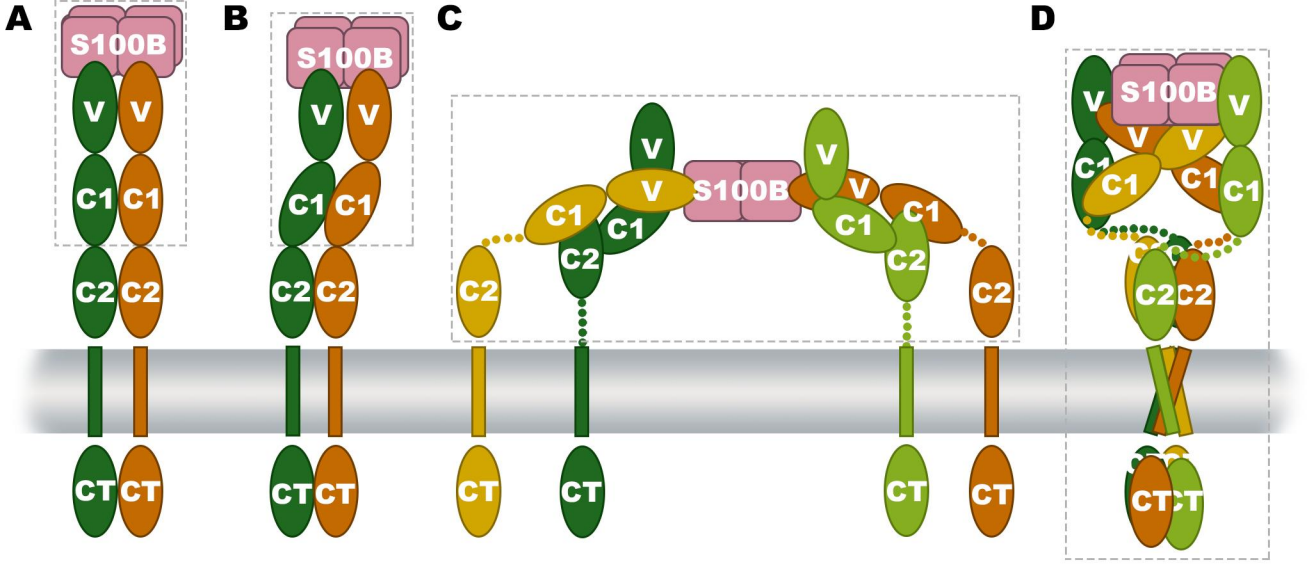
A
S100B
V
V
C1
C1
C2
C2
CT
CT
B
S100B
V
V
C1
C1
C2
C2
CT
CT
C
V
V
S100B
V
V
C1
C1
C1
C1
C2
C2
C2
C2
CT
CT
CT
CT
D
S100B
V
V
V
V
C1
C1
C1
C1
C2
C2
CT
CT